Journal of Sedimentary Research

Journal of Sedimentary Research, 2022, v. 92, 546–569
Research Article
DOI: 10.2110/jsr.2021.028

PARALIC SEDIMENTOLOGY OF THE MUSSENTUCHIT MEMBER COASTAL PLAIN, CEDAR MOUNTAIN FORMATION, CENTRAL UTAH, U.S.A.

RYAN T. TUCKER,[1] CELINA A. SUAREZ,[2] PETER J. MAKOVICKY,[3] AND LINDSAY E. ZANNO[4,5]
[1]*Department of Earth Sciences, Stellenbosch University, Private Bag X1 Matieland, Stellenbosch 7602, South Africa*
[2]*Department of Geosciences, University of Arkansas, 226 Gearhart Hall, Fayetteville, Arkansas 72701, U.S.A.*
[3]*Department of Earth and Environmental Sciences, University of Minnesota, Minneapolis, Minnesota 55455, U.S.A.*
[4]*Paleontology, North Carolina Museum of Natural Sciences, 11 West Jones Street, Raleigh, North Carolina 27601, U.S.A.*
[5]*Department of Biological Sciences, Campus Box 7617, North Carolina State University, Raleigh, North Carolina 27695, U.S.A.*
e-mail: tucker@sun.ac.za

ABSTRACT: **Although intensified work on the volcaniclastic-rich sediments of the fossil-bearing Mussentuchit Member (uppermost Cedar Mountain Formation, Utah) has provided a refined chronostratigraphic framework, paleoenvironmental interpretations remain cryptic. To resolve this, we performed facies analysis and architectural reconstruction on exposed Mussentuchit Member outcrops south of Emery, central Utah, USA. Contrary to previous interpretations (fluvial, lacustrine), we identified a broad suite of facies that indicate that deposition occurred on the landward part of a paralic depocenter, influenced by both distal alluvial and proximal coastal systems. We conclude that the Mussentuchit Member was a sink for suspension-settling fines with most undergoing pedogenic alteration, analogous to the modern coastal plain of French Guiana (Wang et al. 2002; Anthony et al. 2010, 2014). However, this landward paralic depocenter was not uniform through time. Sedimentological evidence indicates landscape modification was ongoing, influenced by an altered base-level (high groundwater table, long residency of water in sediments, shifts in paleosol types, heavier to lighter $\delta^{18}O$, and distinct shifts in relative humidity (ε); common in coastal settings). If the above data is coupled with recent age data, we interpret that the Mussentuchit Member correlates to the S.B. 4 Greenhorn Regression (Thatcher Limestone) of the adjacent Western Interior Seaway to the east. As a landward paralic depocenter, the Mussentuchit would have been sensitive to base-level conditions in response to ongoing tectonic processes pushing the foredeep east, and lower paleo-CO_2 levels coupled with a minor global sea-level fall (brief glacial phase) just before to the Cenomanian–Turonian Thermal Maximum. Altogether, our results not only strengthen linkages in the central Western Interior Seaway, but simultaneously results in novel linkages to near-coeval paralic depocenters across mid-Cenomanian North America.**

INTRODUCTION

A scarcity of contextualized Cenomanian sedimentary successions in the Western Interior has long hindered scientific understanding concerning significant geographic, environmental, and biological transformations (see Kirkland 1998; Mannion and Upchurch 2011; Mannion et al. 2013; Farke et al. 2014; Driebergen et al. 2017; D'Emic et al. 2019; Nesbitt et al. 2019; Zanno et al. 2019). Linkages remain tenuous between the known terrestrial Cenomanian sedimentary successions in the mosaic of isolated sedimentary basins and sub-basins in the Western Interior (Greenhalgh and Britt 2007; Roca and Nadon 2007) as well as between terrestrial sediment successions and transgressive–regressive cycles of the Western Interior Seaway (Kauffman 1984; Steel et al. 2012; Lin and Bhattacharya 2020; Cilliers et al. 2021; Zubalich et al. 2021). Paralic depocenters, common due to vast epicontinental flooding during the Late Cretaceous (Cross and Pilger 1978; Oboh-Ikuenobe et al. 2008; Brown et al. 2013; Colombera et al. 2016; Cavin 2017), are an important tool for resolving linkages between terrestrial and marine sedimentary successions on a local, regional, and global scale, but have been understudied (Cavin 2017; Li et al. 2020; Lin et al. 2020, 2021; Liu et al. 2020). The Cenomanian Mussentuchit Member (uppermost Cedar Mountain Formation, western San Rafael Swell, Utah) is one of several crucial sedimentary successions deposited along the coast of the epicontinental Western Interior Seaway (WIS) during global highstands of the Late Cretaceous. As such, it has the potential to better contextualize and strengthen Cenomanian linkages both across the Western Interior of North American and between terrestrial and marine sedimentary successions globally (Cifelli et al. 1997, 1999; Gillette 1999; Gale et al. 2002; Garrison et al. 2007; McDonald et al. 2012; Makovicky et al. 2014, 2015; Zanno and Makovicky 2013; Frederickson et al. 2017 2018; McDonald et al. 2017; Lowery et al. 2018; Avrahami et al. 2019; Zanno et al. 2019; Kaya et al. 2020; Tucker et al. 2020). Sediments of the Mussentuchit Member were deposited during the Cenomanian (100.5–94.6 Myr) in the eastward-migrating foredeep of the Cordillera Foreland Basin System, east of the Sevier Fold–Thrust Belt (nearly coeval with the Pavant Thrust) (Yingling and Heller 1992; DeCelles et al. 1995; DeCelles and Currie 1996; Cifelli et al. 1997; 1999; DeCelles 2004; Suarez et al. 2012; DeCelles and Graham 2015; Suarez et al. 2017; Tucker et al. 2020). This phase of Sevier foreland development was synchronous with abundant volcanic activity (Phase C; 105–80 Ma) in the western Cordilleran

Published Online: June 2022
 1527-1404/22/092-546

Magmatic Arc, including the Sierra Nevada Batholith, and the more far-flung Idaho and Coast Mountains batholiths (Yingling and Heller 1992; DeCelles et al. 1995; DeCelles and Graham 2015; Tucker et al. 2020). This depocenter was uniquely positioned to accumulate volcaniclastic-rich detritus (Cifelli et al. 1997, 1999; Kirkland et al. 2016; Tucker et al. 2020), and simultaneously preserves evidence of climatic fluctuations, which transpired in this area of the Western Interior of North America (Suarez et al. 2012). Yet, the Mussentuchit Member's specific paleoenvironmental context and linkages to the Western Interior Seaway remain cryptic (Tucker et al. 2020).

Sediments of the Cedar Mountain Formation, including the Mussentuchit Member, are historically interpreted to have been emplaced in an alluvial plain (Harris 1980; Nelson and Crooks 1987; Eaton et al. 1990; Currie 1997), somewhat distant from the Western Interior Seaway (Cifelli et al. 1997, 1999; Goldberg 2000; Garrison et al. 2007). Currently, there is a general lack of consensus as to the specific depositional-system origin, either as a broad-sweeping alluvial system with meandering channels and floodplain fines (Cifelli et al.1997, 1999; Goldberg 2000; Chure et al. 2010; Kirkland et al. 2016) or perennial lacustrine depositional setting (Garrison et al. 2007). These interpreted environments share reported co-occurrences of paleo-taxa, such as *Lonchidion* n. sp. (Kirkland et al. 2016), Yet, similar forms of *Lonchidion* have been documented from the Trinity Group of Texas (Winkler et al. 1990), along with the Arkansas equivalent to the Trinity Group, the Holly Creek Formation (Suarez et al. 2021). The Trinity Group strata (including the Holly Creek Formation) were described as coastal strata, with proximal to distal marine sediments preserved in them. Stable-isotope study of the turtle shells from the Holly Creek Formation (Frucci 2018) suggests that the deposit from which *Lonchidion* comes from is a mixed to brackish-water environment with $\delta^{18}O_{water}$ values calculated as high as $\sim$ –0.5‰ and averaging –3.1‰ VSM. Additional studies also indicate that *Lonchidion* could range from marine, brackish, and even freshwater habitats (Welton and Farish 1993; Noriega 1996; Bhattacharya and MacEachern 2009; Suarez et al. 2012; Kirkland et al. 2013). Therefore, the presence of *Lonchidion* teeth and similar forms in the Mussentuchit Member could indicate mixed-water processes rather than only freshwater processes (Welton and Farish 1993; Kirkland et al. 2013). If the Mussentuchit Member does represent a paralic depocenter, then sedimentation would have been highly sensitive to sea-level changes (T/R Cycles) and provides the potential for novel linkages (Oboh-Ikuenobe et al. 2008; Suarez et al. 2012; Wang et al. 2014; Cavin 2017).

Therefore, the focus of this paper is to contextualize newly described sedimentary successions north of the Fish Lake Plateau and southeast of the Wasatch Plateau along the San Rafael Swell (Fig. 1) to document: 1) the local depositional history for the Mussentuchit Member, 2) reassess the basal contact of the Mussentuchit Member, 3) correlate fossil-bearing strata to key transgression and regression cycles found elsewhere in the Western Interior Seaway, and 4) provide novel stratigraphic linkages to better correlate the Mussentuchit Member across the Western Interior Seaway (WIS). Given the rarity of described muddy Cenomanian rock records along the western shoreline of the WIS, our work would not only provide essential insights into the environmental evolution regionally but would elucidate a broader understanding of geographic and ecological changes in the Cenomanian that can begin to reveal large-scale trends.

BACKGROUND

Initially developed as a foreland basin, the Western Interior Basin (WIB) is partitioned into a mosaic of younger sub-basins related to orogenesis (155–35 Myr) (Roca and Nadon 2007; Giallorenzo et al. 2018). The later phase of deformation included the thin-skinned Sevier Fold–Thrust Belt and the younger basement-core uplifts of the Laramide Orogeny (Willis 1999), exposing older WIB sediments. Relevant to this study is the coeval thrust load (Pavant Thrust), which generated flexural subsidence associated with deformation in the Sevier thrust belt (Currie 2002). Ongoing migration of the forebulge and foredeep influenced the deposition of lower Cedar Mountain Formation eastward of the crustal forebulge, whereas the uppermost Cedar Mountain Formation (Mussentuchit Member) was emplaced in the eastern part of the foredeep (Currie 1997, 2002; Eberth et al. 2006).

The Cedar Mountain Formation is exposed in the central and eastern Utah, with exposure along the Green River, in the Uinta and Henry's basins, along with the San Rafael Swell. The Cedar Mountain Formation is considered coeval with the Burro Canyon Formation in western Colorado, the Cloverly Formation in Wyoming, and the Willow Tank Formation in Nevada (Stokes 1952; Kirkland et al. 1999; Bonde et al. 2008). The stratigraphic expression of the Cedar Mountain Formation is highly variable (Kirkland et al. 1999; Garrison et al. 2007). Kirkland et al. (2016) described lithostratigraphic subdivision of the Cedar Mountain Formation in the San Rafael Swell that includes six regionally variable members (in stratigraphic order): 1) Buckhorn Conglomerate, 2) Yellow Cat Member, 3) Poison Strip Sandstone Member, 4) Ruby Ranch Member, 5) Short Canyon Conglomerate Member, and 6) Mussentuchit Member (Kirkland and Madsen 2007; Hunt et al. 2011; Doelling and Kuehne 2013; Kirkland et al. 2016) (Fig. 1). Individual members are not always present and commonly are laterally discontinuous (Kirkland et al. 2016). Although not all researchers agree with current stratigraphic status; Greenhalgh and Britt (2007) interpreted the Buckhorn Conglomerate, Yellow Cat, and the Poison Strip Sandstone members as coeval units, representing various depositional environments along a transect. Along the westernmost exposures in Central Utah, the Cedar Mountain Formation lacks the Yellow Cat and the Poison Strip members, whereas, the Buckhorn Conglomerate, Ruby Ranch, and Mussentuchit members are consistently present, along with minor exposure of the Short Canyon Conglomerate (Fig. 1). Although in the study area the Cedar Mountain Formation consistently overlies the Brushy Basin Member of the Morrison Formation and is overlain by the Naturita Sandstone, the sedimentological patterns and thicknesses of the aforementioned members and their lower and upper contacts are regionally variable.

METHODS

Fieldwork included detailed facies and architectural element analysis, following the conceptual framework established by Miall (1985, 2016) and modified by Eberth and Miall (1991), Roberts (2007), Reading (2009), Jinnah and Roberts (2011), James and Dalrymple (2010), and Tucker et al. (2017). We employed standard sedimentological techniques and utilized a uniform set of facies codes to consistently describe and interpret the outcrop sections (Miall 2022). Weathered and unweathered color was recorded, using the Munsell Color Chart (2011). This study employed the Bann et al. (2004) hierarchy of bioturbation index (BI) to classify the intensity of bioturbation (BI 0 (none)–BI 6 (intense)) (MacEachern et al. 2012). All facies and stratigraphic correlations are described according to the geographic occurrence in the 7.5–minute (1:24,000) quadrangle topographic map series (Fig. 1).

The expression of transgressive–regressive cycles follows results from Suarez et al. (2012), who used stable-isotope analysis of phosphate oxygen from vertebrate remains to calculate average meteoric-water and river-water isotope composition. Stable oxygen-isotope composition of mammal teeth was then used, combined with meteoric-water proxies (fossilized remains from turtles and crocodylomorphs) to calculate relative humidity, based on an equation for omnivorous rodents (Kohn 1996): $h = 0.16\delta^{18}O_w - 0.26\delta^{18}O_{p\text{-}mammal} + 5.82$ that provides a proxy for relative humidity. Stable isotope analyses for this study were conducted at the Keck Paleoenvironmental and Environmental Stable Isotope Laboratory, housed in the Department of Geology at the University of Kansas. Samples were analyzed on a MAT 253 continuous flow IRMS, connected to a TC/EA (high-temperature conversion elemental analyzer). Detailed sample

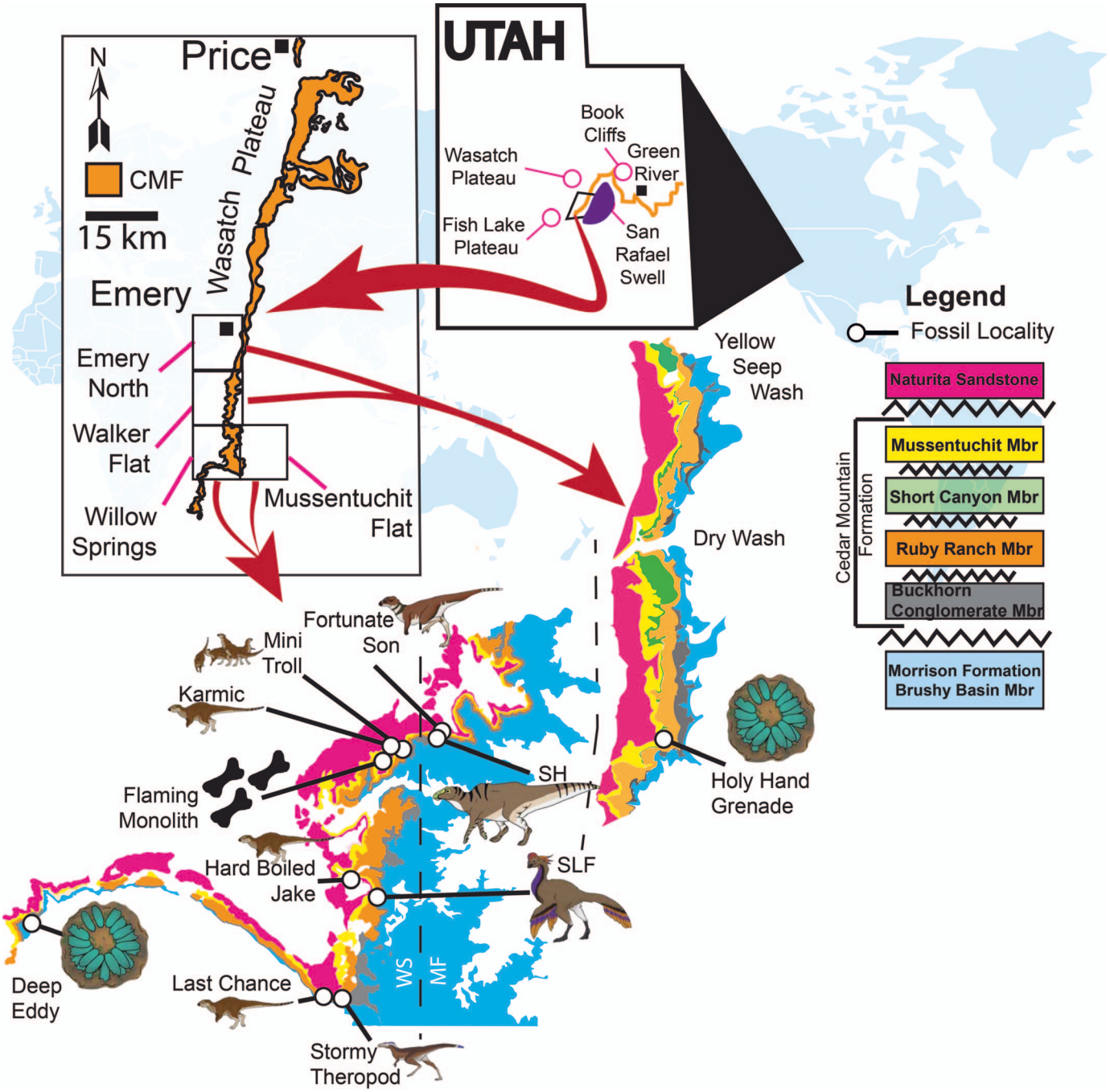

FIG. 1.—Map of Utah displaying the exposed Cedar Mountain Formation across central Utah with inset displaying the western corridor of the exposed Cedar Mountain Formation. The study area is focused in four sections: Willow Springs (aka Cliffs of Insanity), Mussentuchit Flat (Mussentuchit Wash, Tucker et al. 2020), Walker Flat and Emery North (sections based on the 7.5-minute (1:24,000) quadrangle topographic map series). Fossil Sites: 1) Deep Eddy and Holy Hand Grenade, caenaganthid nest; 2) LC, Hard Boiled Jake, Karmic, Orodromine; 3) SLF, Caenagnathidae sp.; 3) Stormy Theropod, *Moros intrepidus* (Zanno et al. 2019); 4) *Eolambia caroljonesa*; 5) Fortunate Son, Early Diverging iguanodontian (Location map and location names modified from Tucker et al. (2020); geological map modified from Hintze et al. (2000).

preparation procedures can be found in Suarez et al. (2012). Samples were converted to silver phosphate (Ag_3PO_4), employing methods of Bassett et al. (2007), where 0.3 mg to 0.5 mg of powder was dissolved in 0.5 m nitric acid; Ca is stripped from the solution, using an ion-exchange reaction with potassium fluoride and potassium hydroxide, converted to Ag_3PO_4 using a silver amine solution. The analysis was monitored through NIST 120c, which returned values of 22.5 ± 0.3‰.

RESULTS

In this study we identified 16 lithofacies (Table 1) and combined with up to five possible architectural elements (Table 2). Once combined, seven repeating sedimentary facies (Fs) were identified and further combined to formulate two facies associations (FAs) (with interpretations; Table 3). For this study, we have divided the Mussentuchit paralic depocenter into two

TABLE 1.—*Lithofacies codes identified in the Mussentuchit Member of the upper Cedar Mountain Formation, modified from Miall (2010), Roberts (2007), and Tucker et al. (2017).*

Facies Codes	Lithofacies	Sedimentary Structure	Interpretation
Gmm	Massive, matrix-supported gravels	Grading	Mass flow
Gmx	Basal gravel rip-ups	Erosional surface, basal gravels, grading	Scouring flow with rip-up clasts, waxing energies
Gst	Gravel, stratified, trough sets	Trough cross bedding	Fluvial in-channel flow
Gsp	Gravel, planar-cross stratified	Planar cross bedding	Channel migration
GSe	Gravel with sand	Crude cross bedding	Mass flow
Sm	Sandy, with or without mud	Massive, void	Void
Sr	Sandy–silty, with or without mud	Ripples	Ripples
Sh	Sandy–silty, with or without mud	Planar lamination	Plane-bed flow
Ss	Sandy–silty, with or without mud	Broad shallow scours	Scour fill
St	Sandy–silty, with or without mud	Troughs	Channel flow with Sand upbuilding
Sl	Sandy–silty, with or without mud	Low-angle cross bedding	Scour fills, chenier ridges
Fl	Clay-rich, with or without silt or sand	Laminated	Waning flood
Fm	Clay-rich, with or without silt or sand	Massive	Suspension settling
Fr	Clay-rich, with or without silt or sand	Ripple cross lamination	Suspension settling with current
C	Coal, carbonaceous mud	Plant, mud films	Stagnating pools
P	Clays	Pedogenics	Paleosol

distinct facies associations: FA1 Distal Paralic or FA2 Proximal Paralic, both occurring (landward) behind the backshore (Fig. 2). Coincidently, the occurrence of these FAs is also stratigraphically dependent with FA2 facies types mostly restricted to the upper Mussentuchit Member. Both weathered and unweathered color codes are presented in Table 4 (Goodard et al. 1995; Munsell Color 2011). Upper and lower bounding surfaces range between 1st and 3rd order, and are based on terminology from Vail et al. (1977) and Miall 2010 (Table 5).

Facies Associations: Descriptions and Interpretations

Paralic Facies Association 1

Facies 1 (F1).—This is the most common F in outcrop, typically composed of the following lithofacies: P, Fm, Fl, Fr, with minor C (Fig. 3A–D). In outcrop, a vast majority of weathered mudstones are a drab gray, dark gray; yet upon closer inspection, F1 can also exhibit light gray, whites, light to medium purple, and mint green. F1 is volcaniclastic-rich, resulting in secondary bentonites with popcorn and haystack weathering (Fig. 3A, B). Individual F1 mudstones are characterized by high amounts of clays and subordinate silts or sands and range from massive (Fm) with internal normal grading or preserved thin lamina (Fl). If exposed, F1 exhibits blocky to pendular fracturing (peds) along with a spheroidal weathering at surface (Fig. 3B). Individual medium- to thick-bedded units are 0.3–2.0 m thick, with a handful of units exceeding 3.0–4.0 m thick. F1 is commonly bounded by 5th-order lower and upper bounding surfaces. F1 is a laterally extensive unit (kilometers) across the mapping area, though more likely this represents multiple laterally related F1s hosted within similar depositional conditions and topographic position (PF). F1s exhibit a poor to moderately preserved A-horizon with a moderate to well-developed B-horizon. If preserved, F1s A-horizon exhibits mud cracks, bioturbation (BI 1) (Figs. 3, 4), minor plant hash, and root traces (Fig. 5A) with rounded glaebules (Fig. 3B–D). The B-horizon exhibits numerous slickensides (increasing in frequency up-section), pervasive mottling (Figs. 3D, 4A, B) (decreasing in frequency up-section), bioturbation (BI 1) (Fig. 3D; *Skolithos*), and frequent evaporites (Fig. 3B–D). Mottling is typically expressed as patches of light gray and dark gray-green. Alternatively, F1 occurs in outcrop as a distinctive mint green (weathered and unweathered) mudstone, which is consistently identified at the base of the lower Mussentuchit Member (within ± 1.0 m of the contact with the underlying Ruby Ranch or Short Canyon members). Although F1 is a major archive of vertebrate fossils, invertebrate and trace fossils remain scarce. Vertical tubes identified as *Skolithos* contain secondary infill (clay) but lacked any surficial character for further identification (Fig. 3D). In the fossil sites Deep Eddy and Last Chance (southern Willow Springs) we have uncovered one disarticulated and one articulated bivalve (unidentified) shell (Fig. 3E); they are seemingly isolated specimens.

F1 Interpretation.—Herein, we interpret F1 to be a gleysol-type paleosol (Retallack 1988; Mack et al. 1993; Al-Suwaidi 2007; Knaust and Bromley 2012; Tabor et al. 2017; Finkl 2019). Gleysols, recently described in Tabor et al. (2017) and Finkl (2019), are characterized by subsurface(s) with distinct redoximorphic features indicative of prolonged, but not permanent water saturation. In F1, we similarly find limited to low-chroma (gray, green) mud cracks, gray-green reduced mottling (pending conditions), and slickensides; however, we have yet to identify ped coatings in outcrop. Structures in the preserved A or B horizons described exhibit subsurface reducing and oxidation shifts (periodic water retention and drying). As mentioned above, in F1, this study identified pervasive diagenetic evaporites, likely pyrite and other iron sulfide–based effluorescenses on freshly exposed surfaces (fracture planes). The presence of this is indicates: 1) much of the Mussentuchit Member is volcaniclastic-rich, and the emplaced ash would be a ready source of iron (Zeng et al. 2018) and 2) seawater is a readily available source of abundant sulfate in marine-influenced deposition such as F1 gleying (Ward 2002; Ludvigson et al.

TABLE 2.—*Architectural elements (lithosomes) identified in the Mussentuchit Member.*

Element	Symbol	Facies	Geometry
Channels	CH	Any Combination	Sheet, concave-up erosional base, commonly bounded by 3rd - to 5th - order surfaces
Laminated Sand Sheet	LS	Sh, Sl, Sp, Sr	Laterally continuous sheets, blankets
Levees	LV	Fl	Wedge to planar, flat-lying
Paralic Fines	PF	Sl-Fl, Fm	accumulation of settling fines, sheet floods, paleosols
Crevasse Splay	CS	Fl, Sl, Sr, Gxb, St	Lenticular, basal 3rd-order surface with rip-ups, internal normal grading; laterally discontinuous

TABLE 3.—*Facies associations identified in outcrop across the Mussentuchit Member. Modified from Miall (2010).*

FAs	Fs		Sediment Scale	Facies Codes	Architectural Elements	Bounding Surfaces	Bioturbation Intensity	Stratigraphic Distribution	Interpretation
FA1	F1		Mud/sand–silt	P, Fm, Fl, Fr, C	PF	5th	1	lower to middle-upper Mussentuchit Mbr	Gleysol development along a paralic plain
	F2		Mud/clay–silt	Fm, Fl, P, C	NA	4th	1–2	lower Mussentuchit Mbr	Plant-rich wetlands
	F3	F3a	Mud/sand/silt/clay	Fm, Fl, and Fr	LS or LV	2nd–4th	0	Both	Small-scale levees or sheet floods
		F3b	Sand/silt/clay	Sm, Sh, Ss, Si, Fl, Gmx	CS	2nd–4th	0	Both	Small-scale crevasse splays
		F3c	Sand/silt/clay	Sm, Sh, Sr, Ss, Si, Fl, Gmx	CH	2nd–4th	0	Both	Small-scale dendritic or ephemeral channels
FA2	F4		Carbonaceous mud, coal	Fl, Fm, C	NA	4th	0	Upper Mussentuchit	Stagnating ephemeral pools and abandoned channels
	F5		Pebbles/sand/silt/mud	GSe, Gmx, Gst St, Sh, SI, Sm	NA	5th	0	Upper Mussentuchit	mixed-process deposit: wave-altered ridges and distal washover fans with subarial alteration (dune) or pre-chenier ridges
	F6		Carbonaceous mud	P, C, Fm, Fl, and Fr	EP	5th	0	Upper Mussentuchit	Histosol (vertic histosol)
	F7	F7a	Sand/clast/mud/silt	St, Sr, Si, Sm, Ss, Sh, and Gmx	CH	5th–3rd	0	Upper Mussentuchit	Large-scale splays
		F7b	Sand/clast/mud/silt		CS	5th–3rd		(One occurrence of muddy channels in lower Mussentuchit)	Large-scale channels

2010, p. 15). The frequency of this paleosol type is stratigraphy-dependent; gleysols are extensive, repeating successions in the lower Mussentuchit Member becoming less frequent to absent in the upper Mussentuchit Member.

Facies 2 (F2).—F2 is more common in the lower strata of the Mussentuchit Member (Fig. 6A) and is composed of the following lithofacies: Fm, Fl, and C. F2 is distinctly light gray, gray-green, to yellowish and black with weathered units displaying a light yellow-gray. F2 is an upward-fining clay-rich to silty mudstones with pervasive plant fragments and plant hash but lacking any discernible lignite or coal. Upper and lower bounding surfaces are typically 4th order, unless hydraulically altered (F3 and F7). Individual beds are extensive, laterally continuous for several hundreds of meters, with bed thickness ranging from 0.4 to 1.5 m. Other than weathering much like F1 and the pervasive floral fragments, F2 does not preserve much internal structure; however, in a few locations lamina (Fl) are present and alternate between coarse and fines. Bioturbation is not well-preserved (BI 1–2), but if present is typically weathered tubes with secondary infill (silt-rich). As with much of the Mussentuchit Member, preservation of bioturbation is poor; yet, in F2 a tentative "Y"-shaped *Thalassinoides* was identified (Fig. 5B) (Kamola 1984). Floral assemblages commonly range from poorly preserved leaves and stems to disseminated carbonaceous flakes (Fig. 6A1).

F2 Interpretation.—Herein, we interpret F2 to be a plant-rich wetland (Dalrymple et al. 2003; Choi and Kim 2006; Hong et al. 2019). Persistent

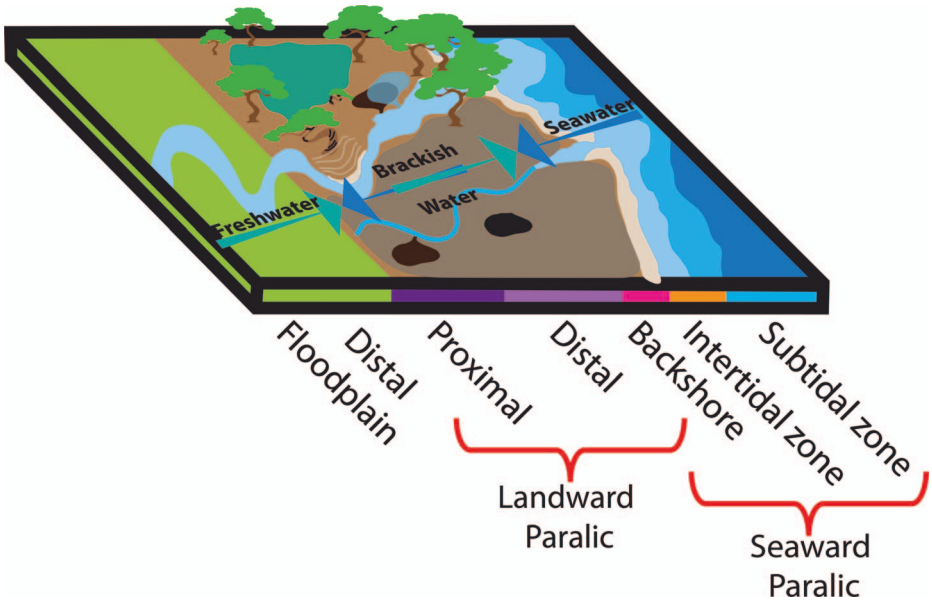

FIG. 2.—Diagram displaying possible depositional zones between the distal floodplain and the coastal margin.

TABLE 4.—*Unweathered and weathered color index.*

Color	Color Code
Light gray	G1 7/N
Medium gray	G1 6/N
Dark gray	G1 4/N
Green gray	10GY 5/2
Light black	10R 6/3
Black	10R 4/3
Light purple	10YR 3/1
Medium purple	10YR 2/1
Mint green	G1 8/2
Olive green	5GY 3/2
Light yellow	5Y 8/4
Yellowish gray	5Y 8/1
Light brown	7.5YR 6/3
Light orange	10YR 8/2
White	N9

TABLE 5.—*Interpreted bounding surfaces based on and modified from Vail et al. (1977) and Miall (2010).*

Group	Time Scale (in yrs.)	Example	Sedimentation Rate (m/ka)	Example	Rank
2	$10^{-5 \text{ to } -4}$	Bedform migration	10^{5}	Ripple	1st
3	10^{-3}	Bedform migration	10^{5}	Seasonal dune increment	1st
4	$10^{-2 \text{ to } -1}$	Bedform migration	10^{4}	Dune	2nd
5	$100–10^{1}$	Seasonal event (10-year flood)	10^{2-3}	Macroform growth	3rd
6	10^{2-3}	100-year flood	10^{2-3}	Macroform (splay, levee, immature paleosol)	4th
7	10^{3-4}	Long-term process	10^{0-1}	Macroform (channel, paleosol)	5th

alternating greenish-gray and yellowish-gray color indicates periodic oxidation and reduction (saturation and drying), interpreted to result from a fluctuating base-level (similar to F1) (Miller and Sigleo 1984; Retallack et al. 1997; Retallack 2001; Tabor and Myers 2015).

Facies 3 (F3).—F3 is moderately common throughout the field area and occurs in two typical geometries and sediment types: F3a muddy sheets or F3b and F3c laterally discontinuous sand-rich or silt-rich muddy lenses (Fig. 6A). F3a is composed of Fm, Fl, and Fr; whereas F3b and F3c are composed of Sm, Sh, Sr, Ss, Si, and Gmx. Both F3a and F3b exhibit similar weathered and unweathered coloration, weathered drab grays to green grays and unweathered dark grays. F3a is clay-rich with subordinate sand and silt content and typified by flat-lying 4th order bounding surfaces. F3a is laminated to thin bedded mudstones that do not exceed 0.3 m thick, with most ranging from 0.05 to 0.1 m. Thicker units (0.1–0.3 m) tend to preserve normal grading (Fm), yet in a handful of units thin laminae (Fl) or asymmetrical ripple cross-lamination (Fr) is preserved. F3a can extend laterally for tens of meters to a maximum of 50 to 60 m. Mud cracks have been observed but are not common. F3b, is muddy; however, a distinct increase of sand to silt ratios was readily noted. F3b can contain basal gravels or coarse sands, along with variable amounts of clay rip-up clasts (Gmx). F3b is laterally discontinuous, thin to medium-bedded units range from $\sim$ 0.2–0.6 m.

Architecturally, F3 can be separable into two basic geometries: 1) sheets (F3a) or 2) lenticular (F3b and F3c). Stacked planar or sheet-like F3a is typically channel adjacent, stacked, and commonly exhibits upwards fining indicative of levee development (LV). Non-channel-adjacent sheets are more likely laterally extensive sheet flow (SF). Lenticular F3b presents as lenticular sandy units with basal gravels mixed with clay rip-ups, both vertical and lateral normal grading with 3rd-order basal surfaces, and crevasse splays (CS). F3c is restricted to small-bodied, concave-up, lenticular, internally graded, thin-bedded units, and channel elements (CH). F3c also infrequently preserves asymmetrical ripple cross-laminated sands and silts or internal small-scale trough cross-bedding.

F3 Interpretation.—We identify F3 as distal alluvial, suspension-settling events across an expansive, low-lying topographic area (Reading 2009). F3a is herein interpreted as laterally extensive, low-energy sheet floods with suspension setting as the major means of sediment emplacement. On the other hand, if F3a is channel-adjacent, it is interpreted as poorly to moderately developed levees. Lenticular F3b units are interpreted as crevasse splays, and concave up F3c units are interpreted as low-energy dendritic channels.

Paralic Facies Association 2

Facies 4 (F4).—F4 is less common, however, in outcrop, F4 is very distinctive. Composed of Fl, Fm, and C, F4 is diagnosed as isolated concave-up, laterally discontinuous lenses of concentrated carbonaceous mudrock (Fig. 6D, E). Upper and lower bounding surfaces are 4th order. Individual beds are generally thin- to medium-bedded ($\sim$ 0.2 to 0.5 m) and laterally pinch out at 10 m. Carbonaceous mudrocks commonly contain high amounts of lignite and disseminated peat fragments, with organic content ranging from 30 to 80%. In lighter units (light gray), poorly preserved leaf and bark fragments may occur.

F4 Interpretation.—Herein, we interpret F4 to be ephemeral (short-lived) wetland pools isolated to low-lying topographic depressions lacking an outlet and are the result of groundwater fluctuations (Johnson and Rogers 2003). In these depressions or abandoned toughs, high-water stagnating pools consist of high amounts of organic matter (McCabe 1987; Reading 2009; Ielpi 2013). F4 signifies mixed deposition of clay and organic material that decayed over the course of deposition. Mostly, F4 lacks sand or silt fractions, indicating a low-energy environment. We interpret these pools to have occurred during higher-groundwater phases, thus filling in topographic lows, and simultaneously accumulating large amounts of organic matter. The presence of internal lamina is rare but present in a few instances (troughs), which indicates that decomposition was infrequently interrupted by low-energy sediment input (Botfalvai et al. 2016).

Facies 5 (F5).—F5 is identified as elongated sand bodies in a handful of localities and is composed of GSe, Gmx, Gst St, Sh, SI, and Sm. In outcrop, F5 is typically unweathered light-gray or faded green-gray and weathered to a light-gray or orange. F5 is atypical for units in the Mussentuchit Member, containing minor amounts of clays. F5 exhibits 4th-order flat-lying to undulating upper and lower bounding surfaces, with beds ranging from 0.15 cm to 1.8 m and can extend laterally for hundreds of meters. F5 sediments range from pebbles and granules to medium silts, with units generally grading normally (Figs. 7, 8A, B). Pebbles and granules vary greatly in rounding and sorting, with a few instances of clast-supported horizons (GSe, Gmx). Typically, basal pebbles grade normally to fine sands or medium silts in discontinuous thick-laminated to thin-bedded flat or troughed horizons (Fig. 7A–C). Thinner units can exhibit wavy-parallel-laminated sands and silts, whereas thicker units exhibit stacked discordant internal laminae (bundled upbuilding), and irregular to undulating laminae (chevron upbuilding) are present (Figs. 7B, C, 8A, B). Field observations thus far have identified a single isolated lenticular "shelly"–sandy sandstone bed with disarticulated to fragmented oyster

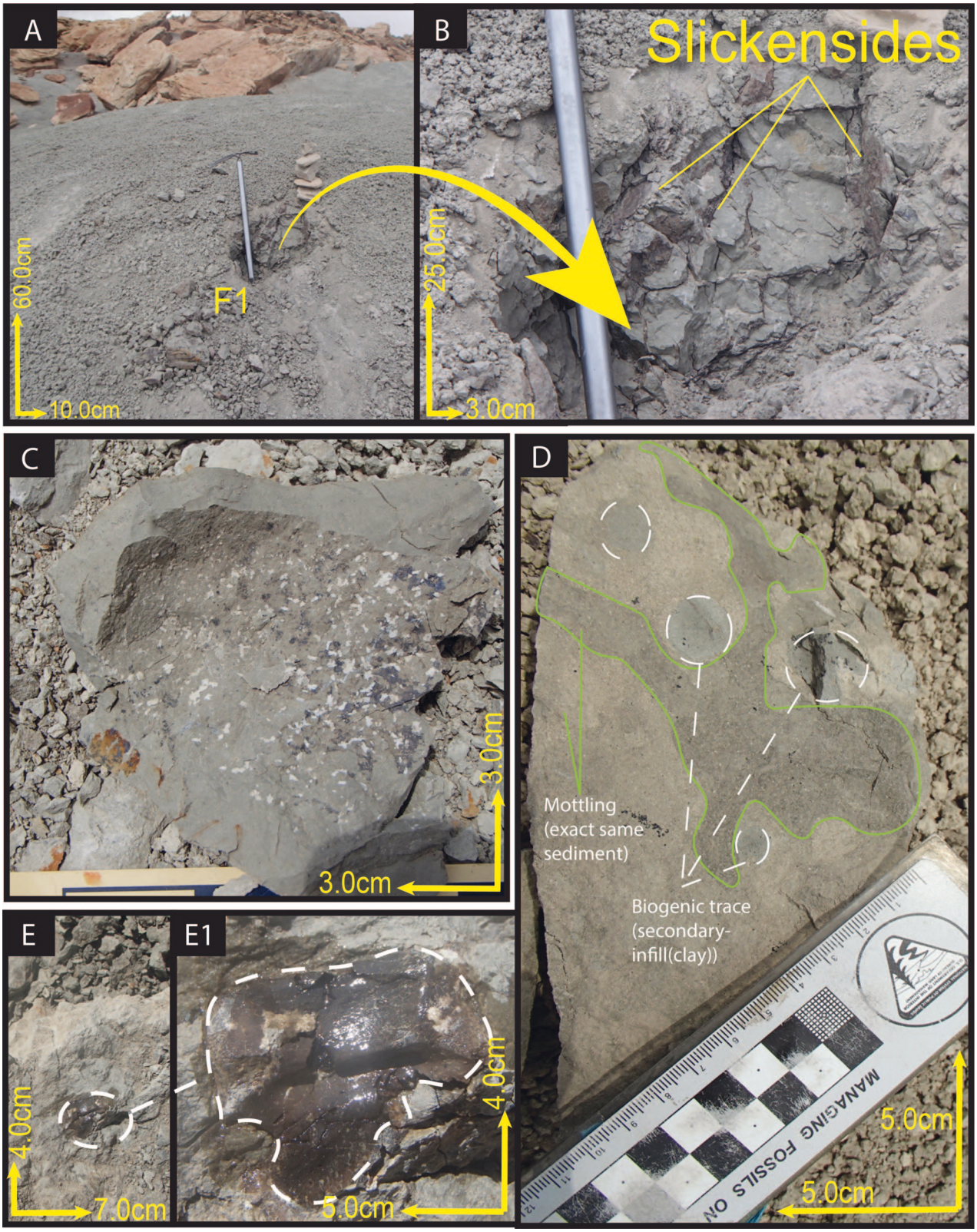

FIG. 3.—**A)** F1 glaysol lacking carbonaceous fragments in the lowermost upper Mussentuchit. **B)** Zoomed in from Part A, F1 gleysols with slickensides in the B-horizon. **C)** Example of disseminated plant films and likely pyrite or other iron sulfide-based effluorescenses on exposed surfaces. **D)** Typical mottling and *Skolithos*-type bioturbation traces (secondary clay infill) near to the fossil site Deep Eddy. **E**, **E1)** Partial bivalve shell found at the Deep Eddy fossil site.

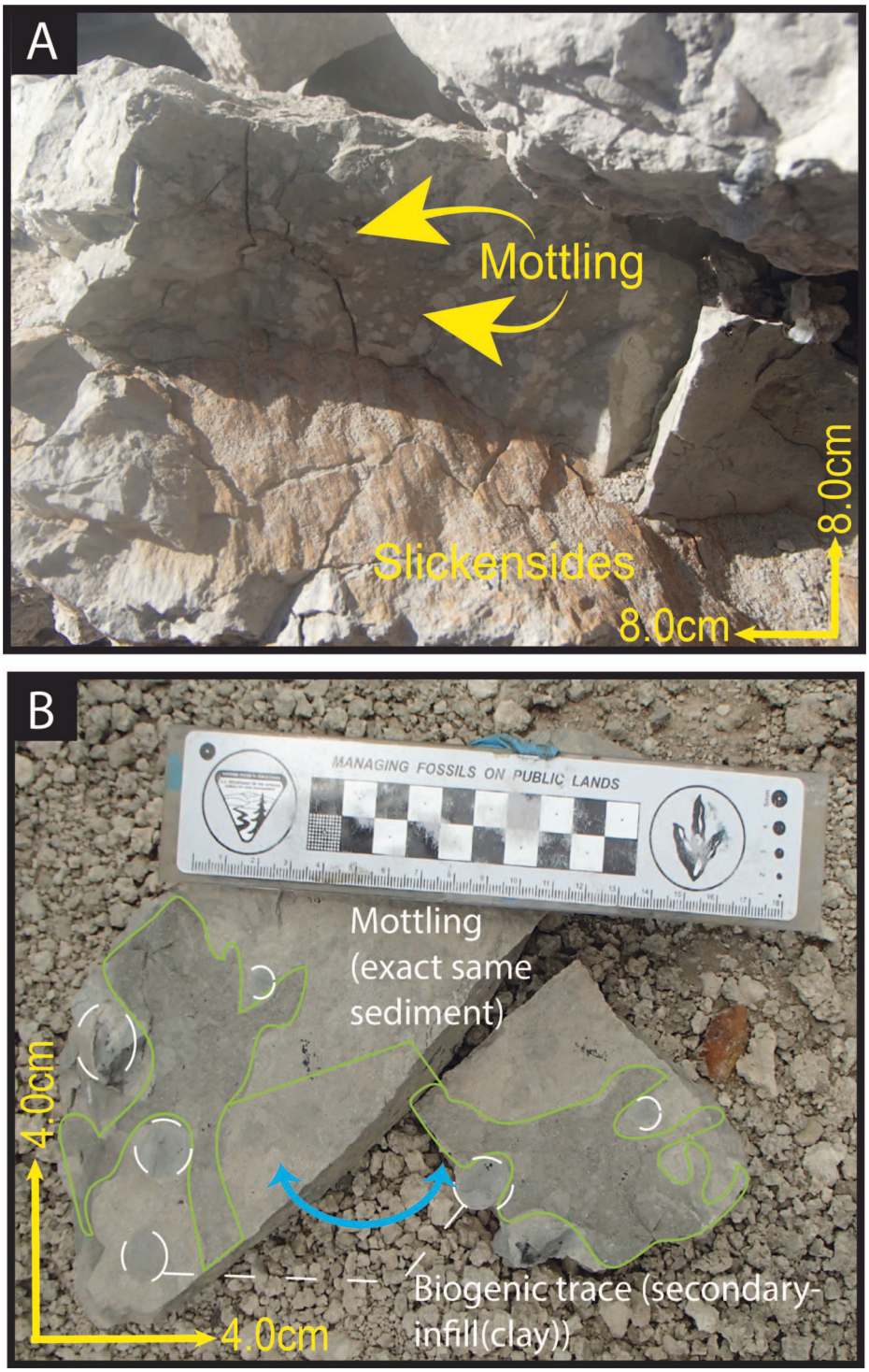

FIG. 4.—**A)** Example of co-occurring mottling and slickenside in the uppermost lower Mussentuchit member. **B)** Example of co-occurring mottling and biogenic traces (detailed image of Fig. 3D) with dark gray to greenish gray and light gray mottling. Blue arrow indicates that sample was split in half.

(molluscan) remains (also noted in Garrison et al. 2007, p.472). The individual shells and shell fragments are randomly oriented, and no escape structures were identified. The sandy matrix is similar to that of other F5s (Fig. 8C, C2, C3).

F5 Interpretation.—The vertical building of rather coarse sediment is interpreted to represent emplacement by a combination of waves or tides in combination with wind (Otvos 2000; Pemberton et al. 2012). We interpret that these clastic and coarse grains accumulated during storm events that push sediment landward, behind the foreshore and backshore. Finer sediment was thereafter modified, likely by wind. This would indicate that F5 is a mixed-process deposit (Pemberton et al. 2012). In the least, F5 is herein interpreted as relict wave-built gravelly–sandy ridges modified to dunes. However, these gravel–sand bodies are sandwiched between muddy units of F1 and F2, typical of distal washover fans, sandflats, or pre-chenier ridges that are driven landward and above the supratidal zone (Pemberton et al. 2012; Fan et al. 2013; Morales et al. 2014; Otvos 2019a, 2019b). An isolated stratum of oyster (molluscan) shell hash (disarticulated to

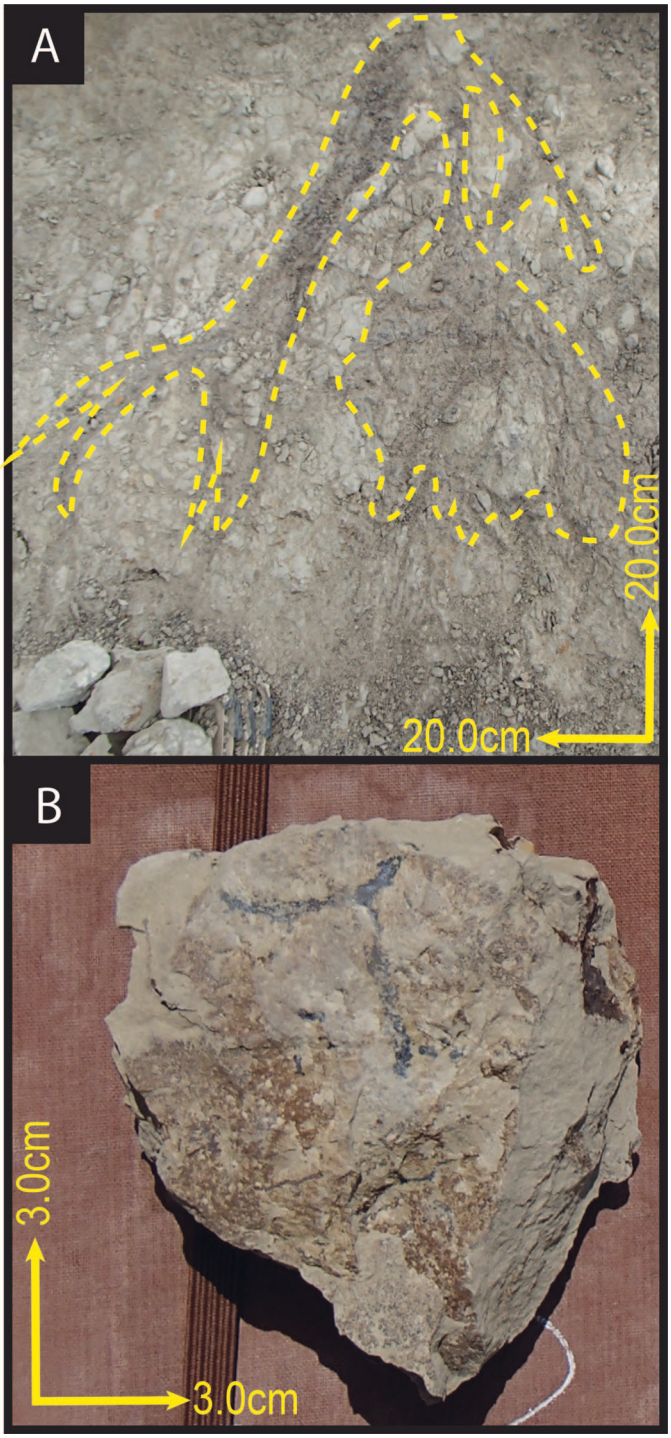

FIG. 5.—**A)** Complex root traces in F1 gleysols; traces are preserved as carbonaceous-rich muds in an outward-expanding and bifurcating structure. **B)** Y-shaped *Thalassinoides* trace.

fragmentary) lacked any evidence of escape structures, therefore indicating a singular emplacement event (storm surge), yet the assemblage would have been time-averaged and parautochthonous in nature.

Facies 6 (F6).—F6 is composed of the following lithofacies: P, C, Fm, Fl, and Fr. In outcrop, unweathered mudstones are typically light-brown, light-gray, or light-dusty-black; weathered units exhibit light gray and black with infrequent light yellow and light orange (Fig. 9). F6 is typified by laterally discontinuous to laterally continuous carbonaceous muds with co-occurring slickensides, pervasive plant hash, root traces, and less frequent mottling (Fig. 9B1). F6 exhibits blocky to platy fracturing. Individual medium- to thick-bedded units ranged from 0.2 to 1.5 m thick. Thin lenses of lignite have been identified; however, carbonaceous mudstones contain unidentifiable plant hash. In F6 both O and B soil horizons are fairly well preserved, with the O-horizon preserving invertebrate bioturbation (BI 2–3), root traces (adventitious prop root-like, to adventitious roots from a trunk-like to monopodial branching-like patterns) (Gill and Tomlinson 1977; Retallack 1988), root casts (near to Deep Eddy ~ 100 m; mangrove-like), mud cracks, and small-node or rounded glaebules (Fig. 3). The defined "B-horizon" preserves pervasive slickensides and distinctly less diagenetic evaporites and mottling than F1 (Fig. 3).

F6 Interpretation.—Based on the above characteristics, we find it reasonable to identify F6 peaty sediments and co-occurring pedogenic structures as a histosol-type to vertic-histosol type paleosols (Brewer and Sleeman 1964; Whybrow and McClure 1980; Retallack 1988; Galli 1991; Mack 1993; Gingras et al. 2012; Knaust and Bromley 2012). Concentrations of organic material (OM) are predominantly accumulating in the O-horizon with decreasing concentrations in the underlying B-horizon. B-horizon is readily recognizable with pervasive shrink-and-swell structures (slickensides). Based on the concentrations of OM, these particular histosols likely can be recognized as fibrists to hemists (Eswaran et al. 2005). Thus far, histosol-type paleosols of any variation are restricted to the upper Mussentuchit Member.

Facies 7 (F7).—F7 typically preserves St, Sr, Si, Sm, Ss, Sh, and Gmx (Tables 1, 3). F7 units are characterized by sandstones to sandy siltstone units with minor clays that commonly exhibit internal normal grading. Individual sand–silt bodies range from massive (Sm) and structureless to having well-preserved internal structures that include 1) cross-bedding sets (St, Sp) that are commonly 0.3–1.5 m thick (angle of repose commonly ranges between 8 and 12°) or 2) ripple cross-lamination to planar cross-lamination or planar cross-stratification (Sr, Sh, Ss) (Fig. 10). Trough cross-bedded sandstone occur in two distinct patterns, with mud drapes in the lower Mussentuchit Member, and without mud drapes in the upper Mussentuchit Member (Fig. 10C–E). F7 represents thick-bedded sandstone bodies not exceeding 2.0 m thick that typically extend laterally for significant distances, in some cases kilometers. F7 is typified by basal 5th- to 3rd-order erosional bounding surfaces and 4th-order flat-lying to erosive upper bounding surfaces. Where basal 5th-order surfaces are erosional, intraclast (clay rip-ups), or small-gravel to granular sands (Gmx), are observed in the lowermost 0.01–0.10 m of the units.

Diverse architectural elements are recognized (*sensu* Miall 2016), including channel-associated elements: channel elements (CH: F7a) (Fig. 4) and crevasse splays (CS: F7b). CH elements range in thickness from 0.4 to 2.0 m and extend laterally for 10.0 to 40.0 m (sheets can laterally extend for several kilometers) to laterally discontinuous multilateral trough-bedded sandstones (Fig. 10A, B). Large-scale CH in multilateral upbuilding is rare in outcrop, with only a handful of localities documented thus far. CS ranges in scale from small-scale lenticular sandstone (~ 0.4 m thick by 5.0–8.0 m in lateral extent) to large-scale lenticular sandstone (~ 1.0–1.5 m thick by 10.0–15.0 m in lateral extent), both exhibiting basal Gmx, along with co-occurring rip-up clasts and redeposited fossil material (e.g., fossil-assemblage site Flaming Monolith).

F7 Interpretation.—F7 represents distal in-channel fluvial deposits or adjacent-to-channel splays. Large-scale macroform elements identified in outcrop, particularly CH and CS, are all consistent with this interpretation

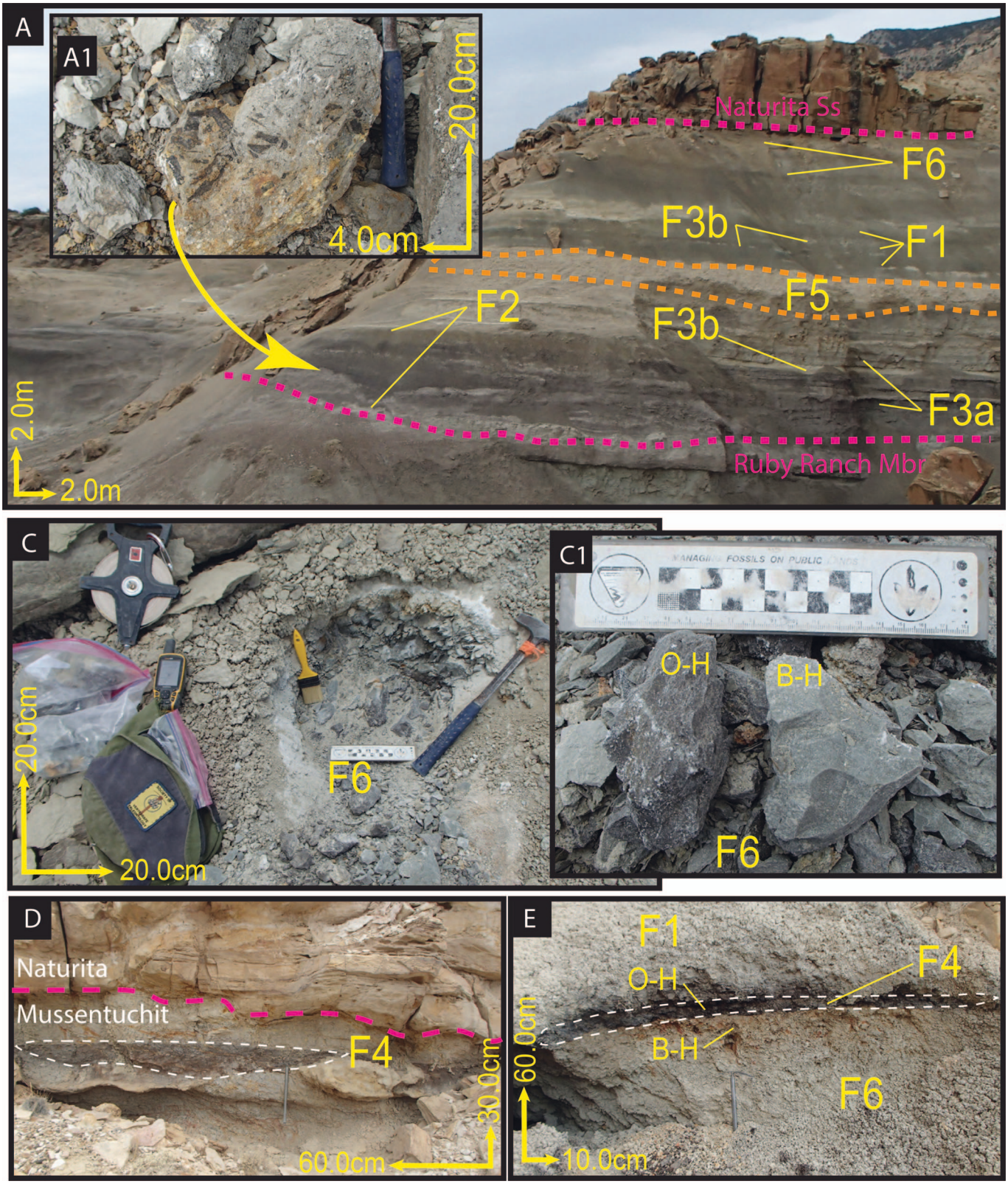

FIG. 6.—**A**, **A1)** Cliff-exposure of the underlying Ruby Ranch Member, Mussentuchit Member, and overlying Naturita Sandstone Member with key facies indicated, F2 wetlands facies and preserved plant hash. **B**, **B1)** Observed histosol in the middle upper Mussentuchit member with a distinct carbonaceous mudrock interpreted as the O-horizon (O-H) and the underlying B-horizon (B-H). **C)** Concave-up, abandoned dendritic channel (F4) with carbonaceous mudrock infill along with secondary alteration to vertic-histosol with pervasive underlying slickensides. **D)** Ephemeral pool (F4) with input of stagnating waters and high amounts of organic materials with secondary alteration to vertic-histosol with pervasive underlying slickensides.

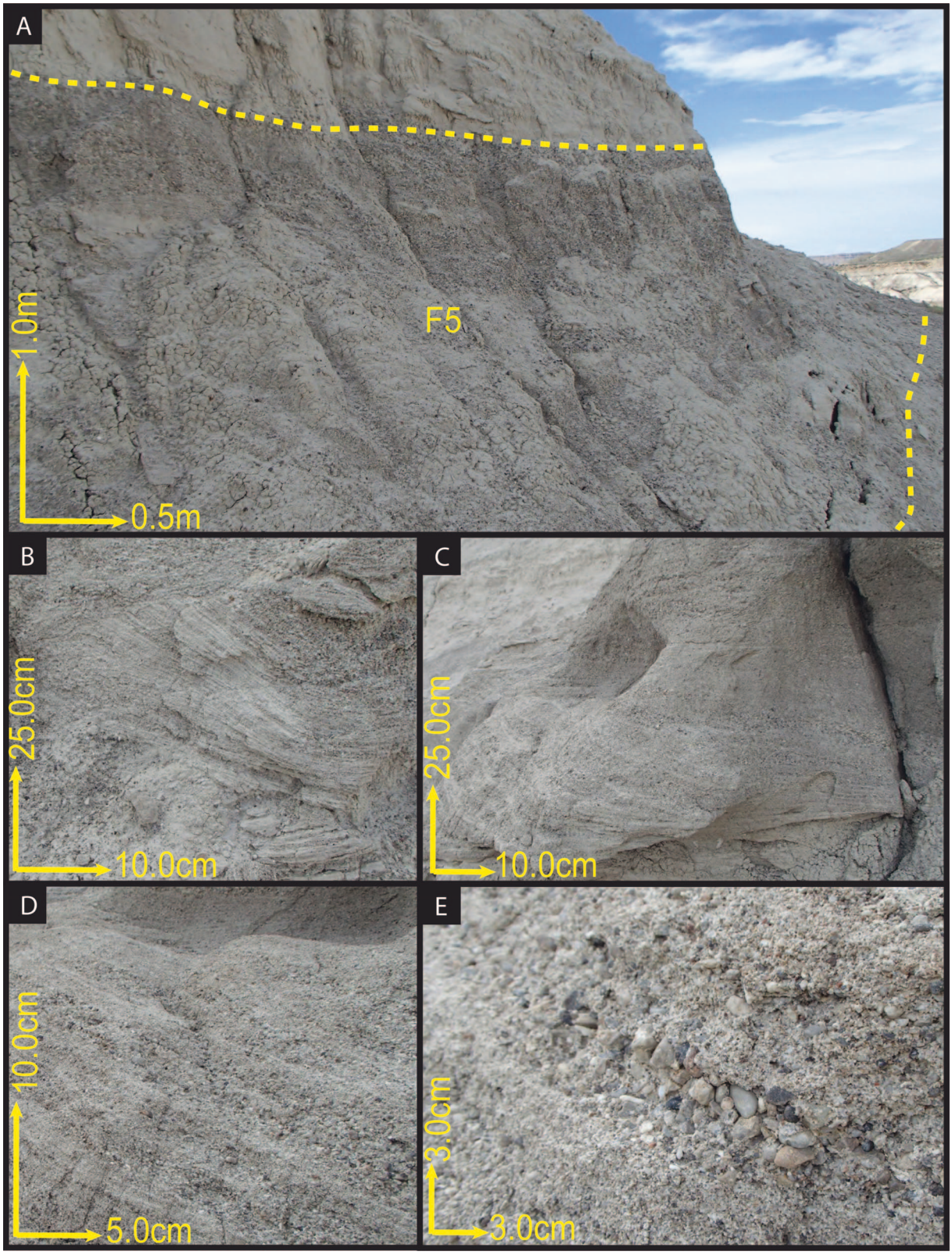

FIG. 7.—**A)** Exposure of ± 2.0 m section of F5, interbedded between an overlying and underlying F1. **B)** Trough cross-bedding and truncated laminae of stacked dunes. **C)** Trough cross-bedding and repeating fining upwards from pebbles to sands. **D)** Close-up of thin-bedded to laminated units, grading normally from pebbles to sands. **E)** Closeup of bedded pebbles and sands lacking the characteristic muds of the Mussentuchit Member.

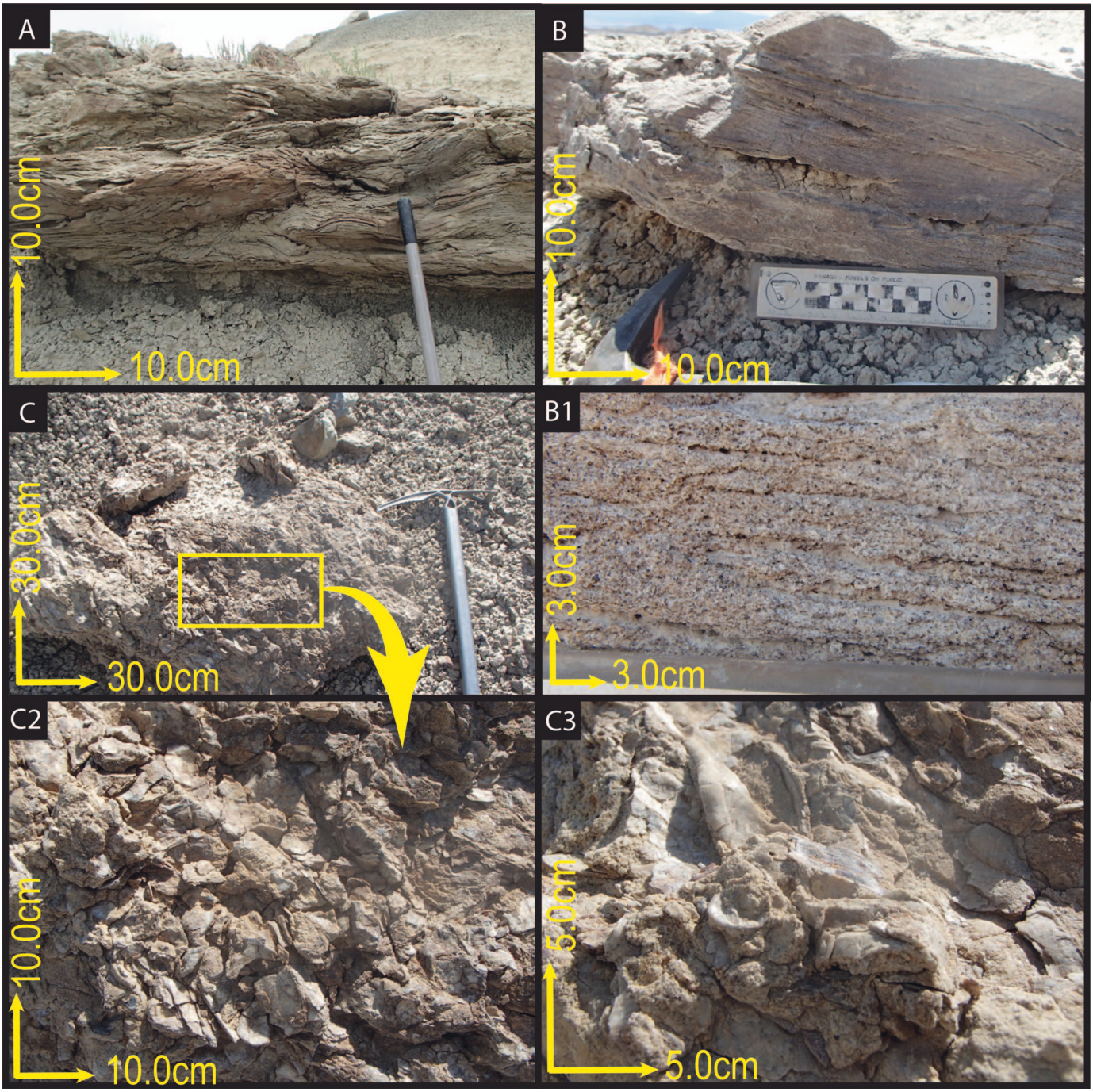

FIG. 8.—**A**, **B)** Isolated examples in the Mussentuchit Flat of sandy, trough cross-bedding and truncated laminae of stacked F5 dune-like or pre-chenier structures; B1 displays close-up of sandy fabric. **C)** Laterally discontinuous sandy-shell hash horizon. **C2)** Randomly oriented and disarticulated to fractured nature of the shells in this accumulation. **C3)** Close-up of the oyster-like (molluscan) remains, also noted by Garrison et al. (2007).

(Fielding 2006; Miall 2014). In the lower Mussentuchit, channel elements are limited to a handful of outcrops, mainly in the southern area of Willow Springs or north in Walker Flat. Here, multilateral channel complexes are identified and interpreted as distal fluvial (river mouth) systems (Miall 2014). In the southern Willow Springs, it should be noted that in the lower Mussentuchit Member, trough-bedded sandstone can exhibit mud drapes (interbedded muds) interpreted as waning energy and suspension settling due in part to tidal influx (bidirectional sedimentation) (McIlroy et al. 2005; Facies 3a).

Revised Stratigraphy

The variation in thickness (~ 18.0–40.0 m) of the Mussentuchit Member (along with the underlying members) is linked to the local anticline (Willow Springs) and syncline (Willow Springs and Mussentuchit Flat) along with regional downcutting by the overlying Naturita Sandstone (in agreement with Eaton et al. 1990 and Garrison et al. 2007). In the southernmost Willow Springs and Mussentuchit Flat (north of the Last Chance Desert), a dip is observed to be steepest at ~ 40° with a strike

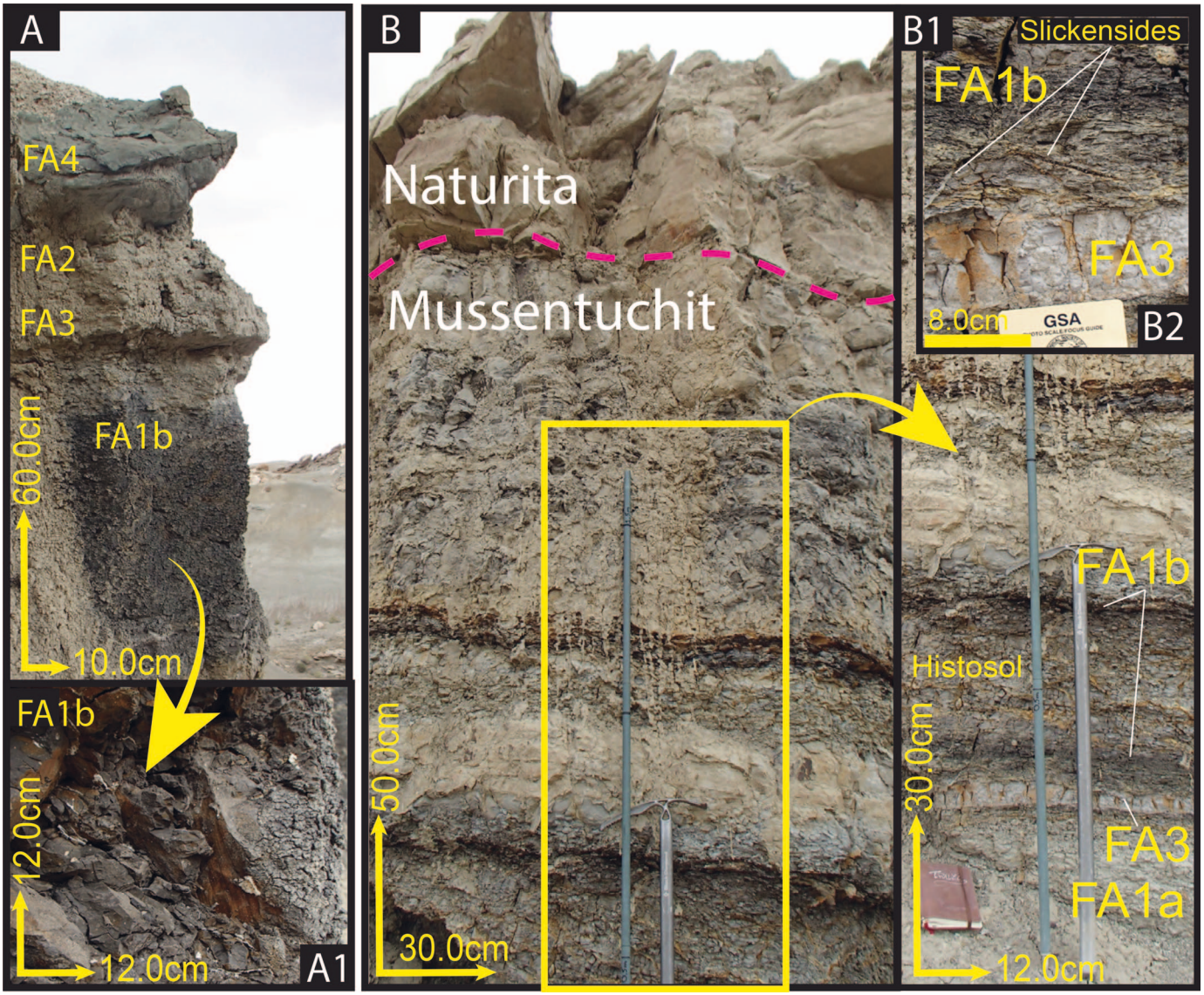

FIG. 9.—Images display the variety of histosol-type paleosols occurring in the upper Mussentuchit Member.

roughly 202–206° SW and 280–284° WNW. In the central and northern mapping areas (Willow Springs, Mussentuchit Flat, Walker Flat, and Emery North, the Mussentuchit dips gently at ~ 4–8°, with a strike between 263–266° WSW and 273–275° W, which is roughly in agreement with the regional geological map (Utah, USGS Map Series). Farther north, the Mussentuchit thins and at some distance is absent from the outcrop of the Cedar Mountain Formation. Field observations are in near agreement with Kirkland et al. (2016); however, local variation is high, and key boundary markers used by Garrison et al. (2007) are inconsistent with our own observations.

Pending location, the lower contact and underlying unit to the Mussentuchit Member is variable (Fig. 11). For central and northern Willow Springs and Mussentuchit Flat mapping area, the Mussentuchit unconformably overlies the Ruby Ranch Member of the Cedar Mountain Formation, with a variably present pebble lag (Fig. 11A, B). Alternatively, at southern Willow Springs and Walker Flat, the Mussentuchit and Ruby Ranch members are stratigraphically separated by the Short Canyon Conglomerate (Fig. 12A). Based on field observations, we reassess the basal contact of the Mussentuchit Member as: 1) *if the Short Canyon is present*, the abrupt absence of a bedded oligomictic paracongomerate and the first occurrence of bentonitic mint green and gray mudrocks (Fig. 12A); or 2) *if the Short Canyon is absent* (Fig. 12B), the contact is indicated by the abrupt loss of pervasive carbonate nodule drapes, a possibly present pebble lag, and the distinctive first occurrence of bentonitic mint green and gray mudrocks ~ 2 m above a trough cross-bedded channel sandstone (if present; originally placed in the basal Mussentuchit Member by Garrison et al. 2007) (Fig. 11A, B). Herein, we also extend the occurrence of the Short Canyon Member to be present in the southern Willow Springs Mapping area, not documented on current geological maps. Throughout the study area, the uppermost Mussentuchit Member is regionally overlain, and distinctly downcut, by the extensive Naturita Sandstone (Eaton 1990; Carpenter 2014).

The lower Mussentuchit Member ranges in thickness from ~ 8.0 to 18.0 m. In the Willow Springs and western Mussentuchit Flat, the lower contact is diagnosed with the abrupt lack of any carbonate nodules coupled with the occurrence of a bentonitic mint green F1 (Fig. 11A1, 12B), roughly 1.0

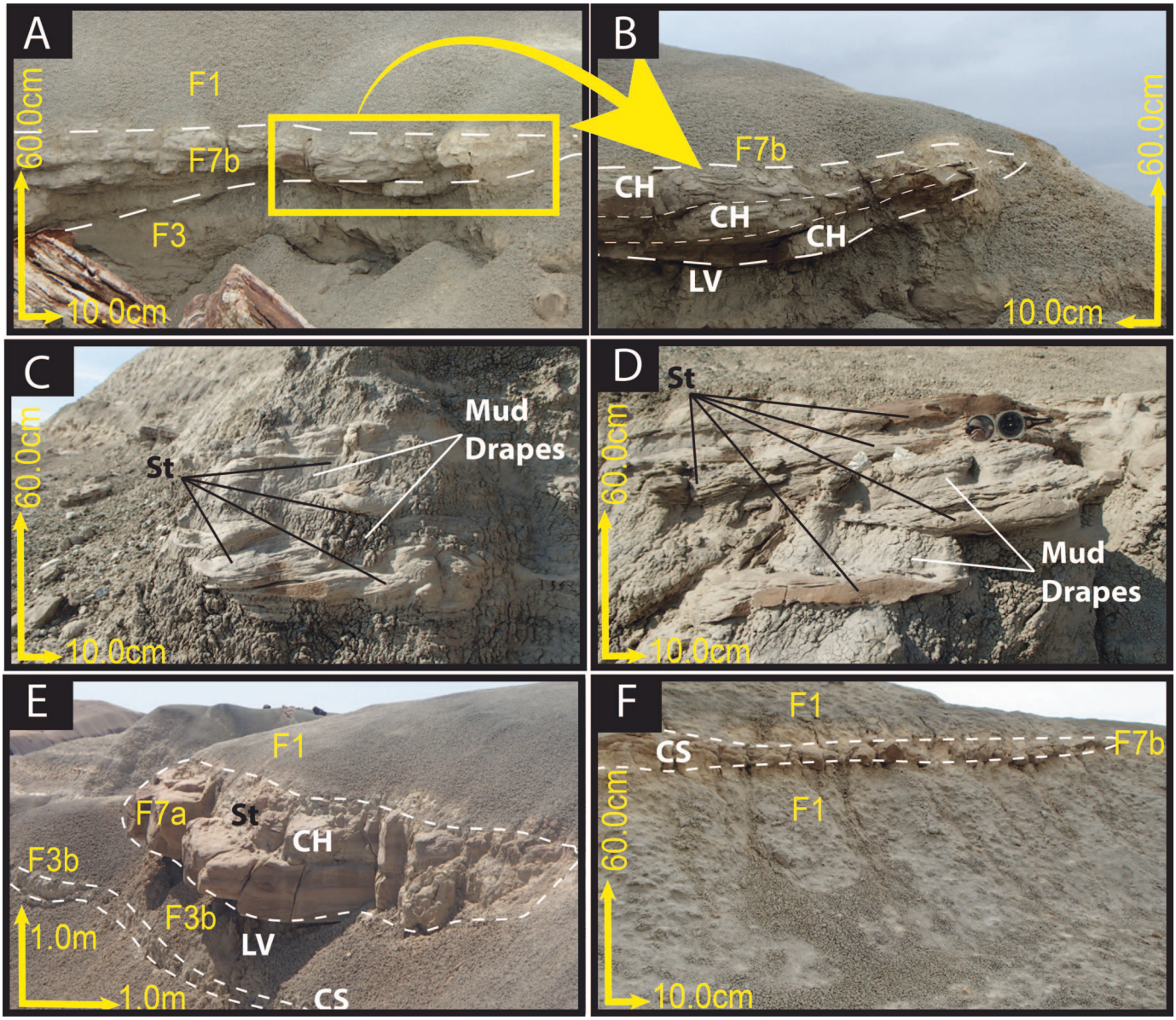

FIG. 10.—**A, B)** Infrequent occurrence of multilateral channel sandstones in the upper Mussentuchit Member in the southernmost area of Willow Springs near to the fossil site HBJ (Part B is a close-up). **C, D)** Examples of the mud-draped trough cross-bedding (bidirectional flow) observed in the lower Mussentuchit Member in the southern mapping area of Willow Springs. **E)** Example of a thick-bedded trough cross-bedded sandstone exhibiting larger-than-normal channel architecture with underlying levees in the upper Mussentuchit Member of the southern Willow Springs mapping area. **F)** Large-scale laterally discontinuous crevasse splay (F7).

m above the contact (Fig. 12A, B). The upper contact of the lower Mussentuchit Member is diagnosed by the occurrence of the first major laterally continuous sandstone (F5), typically 1.0–1.5 m thick. Internally, the lower Mussentuchit Member is diagnosed by the large amount of clay-rich muds with subordinate silts and sands (F1, F2) and minor sand bodies (F3). Units are typically dark gray, mint green (Fig. 12A, B), light purple, or light black, with most weathering to drab gray.

The upper Mussentuchit Member ranges in thickness from 6.0 to 18.0 m (Fig. 12A, B). The lower contact is diagnosed by the persistent sandstone bench (F4) in the "medial" Mussentuchit Member (Fig. 6A, 12A, B). This significant stratigraphic marker bed typically exhibits two distinct patterns: 1) a well-defined olive-green trough cross-bedded sandstone generally ~ 1.0–1.0 m thick (F7) or 2) bedded gravel–sand with variable internal structure (F5), generally ~ 0.8 m thick. Trending north to the Walker Flat and Emery North mapping areas, the middle sand bench marker is harder to diagnose due to the more frequent occurrence of channel elements, and we strongly advocate that total thickness needs to be considered in these areas. Internally, the upper Mussentuchit Member is diagnosed by its greater degree of heterogeneity in both sedimentary characteristics and preserved structures. Sediments are muddy, but to a large degree contain higher percentages of sand or silt (remaining volcaniclastic-rich). The frequency of sandstones and siltstones with subordinate amounts of clay also increases in the upper Mussentuchit Member. Units are typically dark gray, gray, light brown, or light black, weathering to a drab gray. Overall thickness of the upper Mussentuchit Member is variable, trending north as overall thickness decreases to the point of its absence north of J.J. Reservoir, Utah (Kirschbaum and Schenk 2012, their Fig. 5, p. 7).

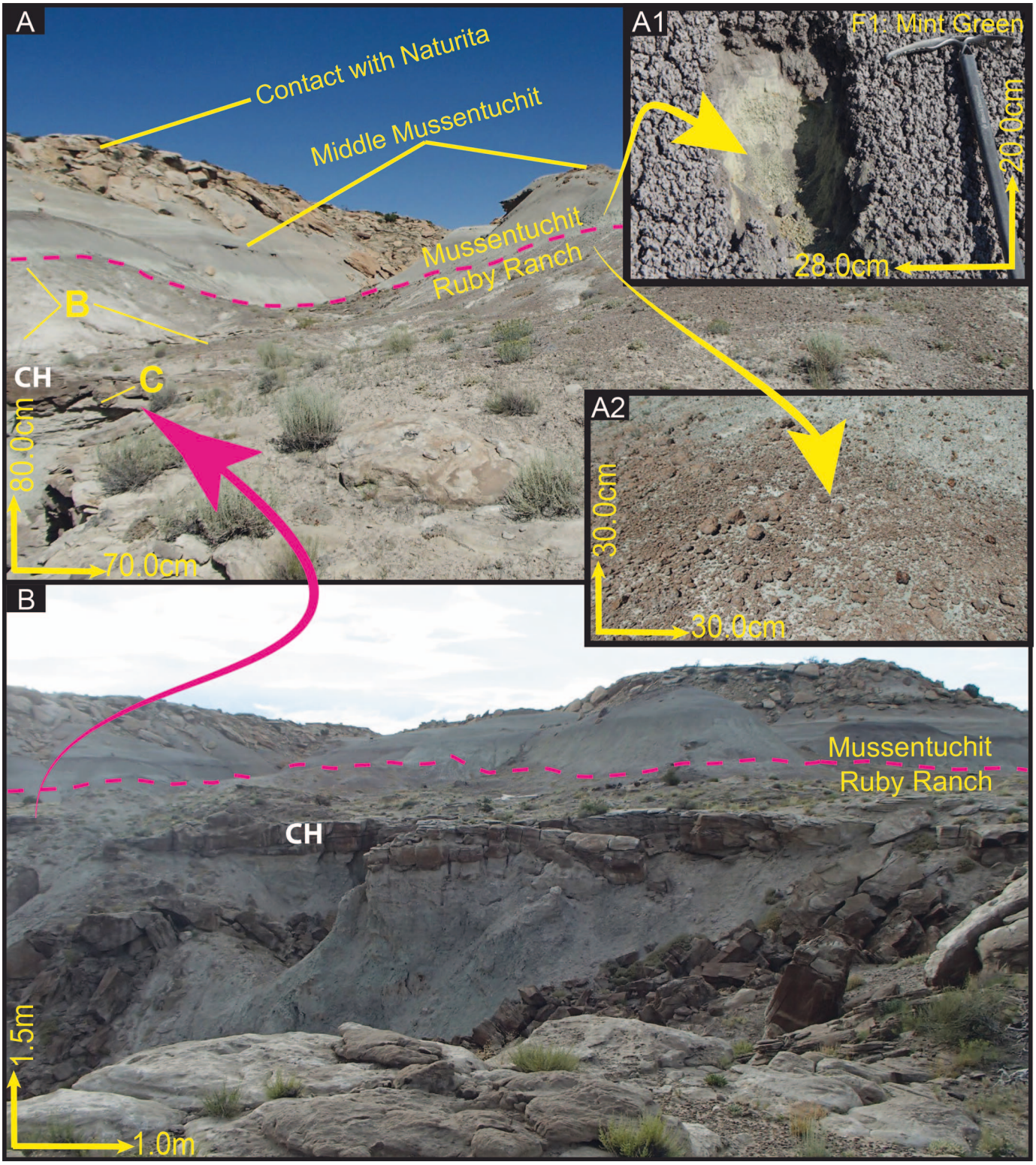

FIG. 11.—Example of contact between the uppermost Ruby Ranch Member and the lower Mussentuchit Member. **A)** Evidence of Ruby Ranch carbonate nodules above the channel sandstone originally interpreted to be in the basal Mussentuchit Member (Garrison et al. 2007). **A1)** Example of mint green F1 mudrock above the interpreted contact. **A2)** Example of the abrupt loss of carbonate nodules just below the interpreted contact. **B)** Zoomed-out image of Ruby Ranch channel sandstone below the contact with the overlying Mussentuchit Member.

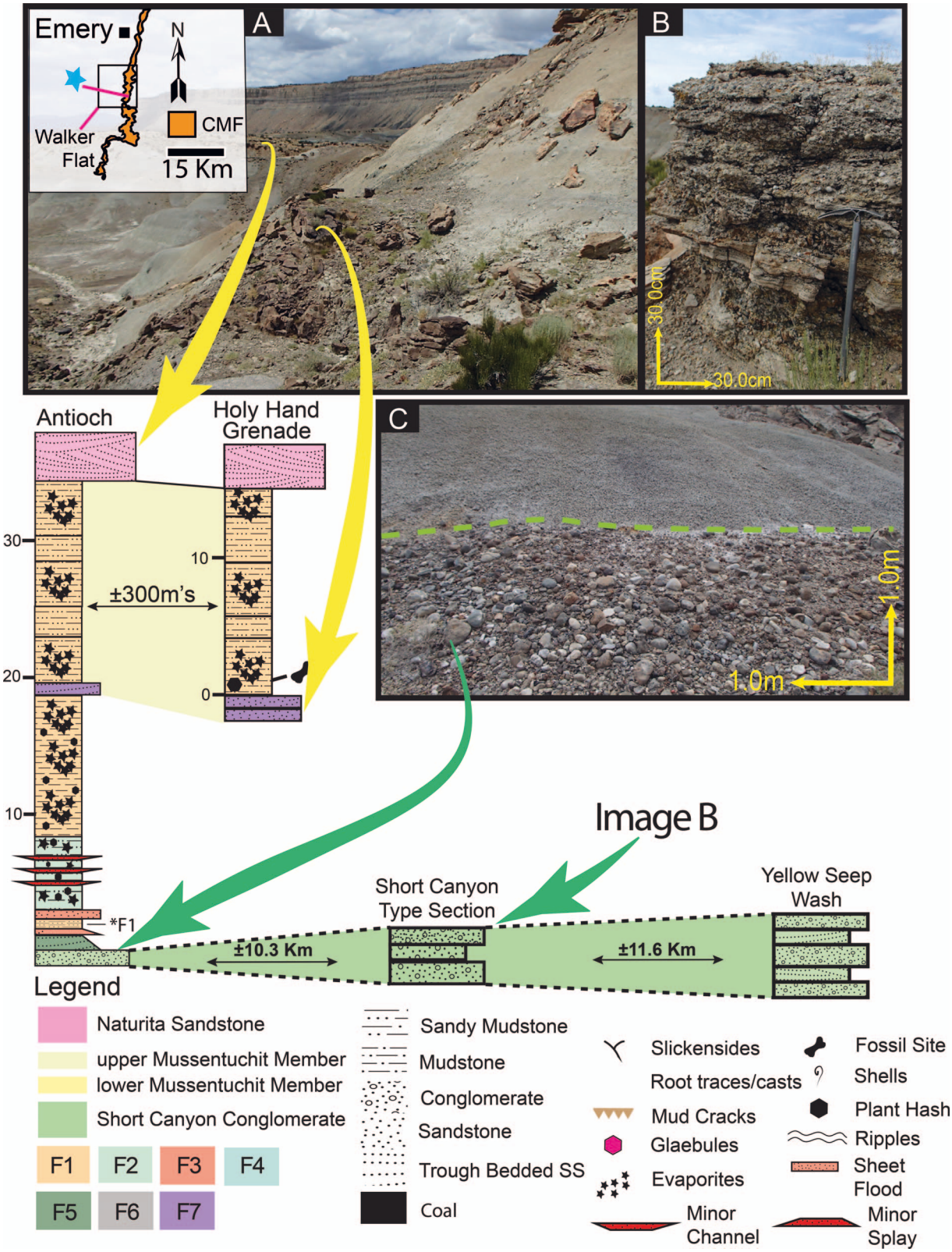

FIG. 12A.—Lithostratigraphic cross-sections of Walker Flat including the Short Canyon Conglomerate (thickening northward). **A)** Examples of outcropping upper Mussentuchit Member in the southern Walker Flat. **B)** Thick-bedded Short Canyon Conglomerate oligomictic paraconglomerate. **C)** Example of pebble lag between the uppermost Ruby Ranch Member and lowermost Mussentuchit Member. F1* denotes the mint green F1 near the basal contact.

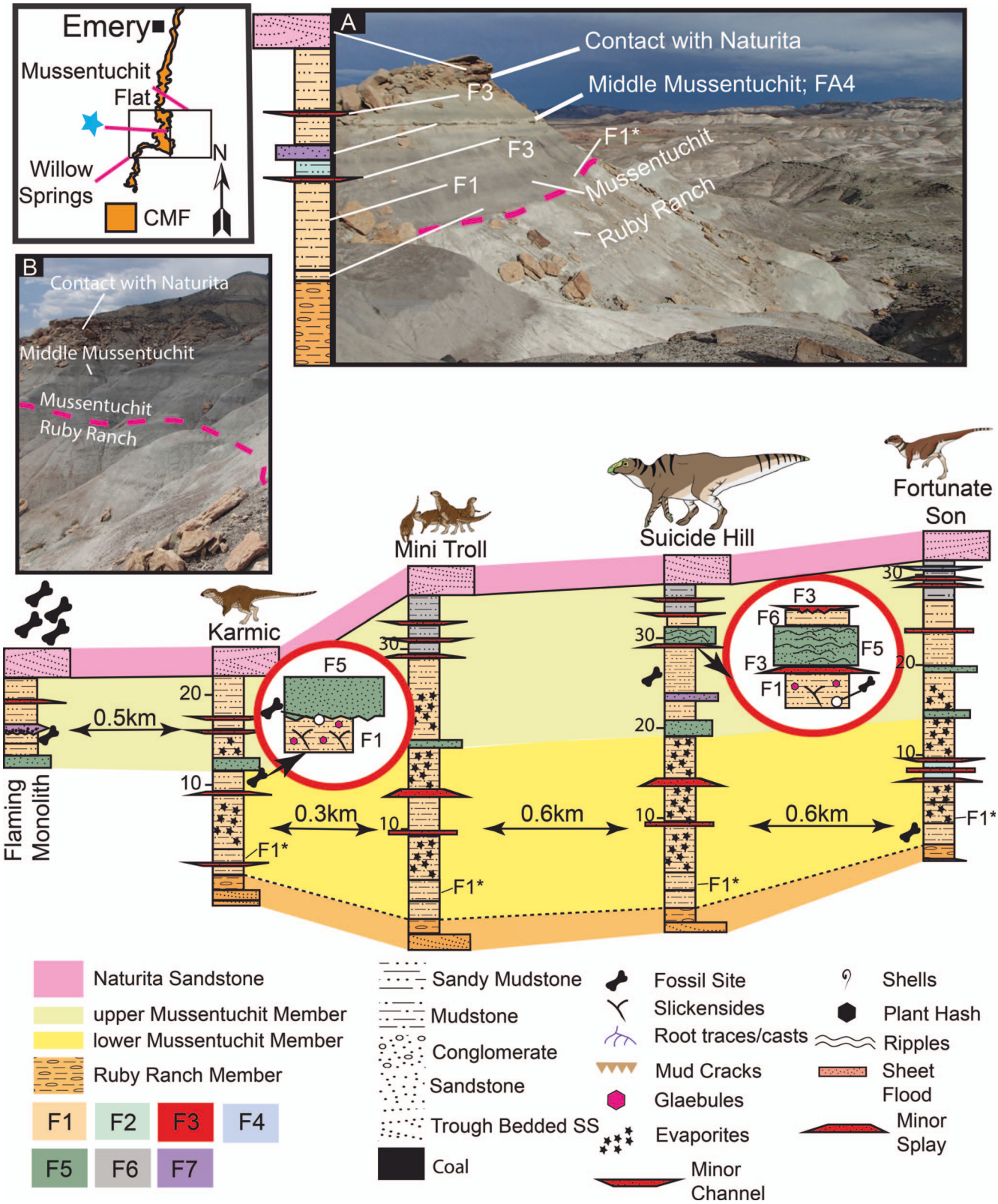

FIG. 12B.—Lithostratigraphic cross-sections of south to the central portion of Willow Springs and Mussentuchit Flat. **A)** Exposed Mussentuchit Member in the Mussentuchit Flat displaying key stratigraphic marker beds including the middle sandstone. **B)** Example of exposed Mussentuchit Member in the central Willow Spring, with the underlying Ruby Ranch Member lacking the uppermost channel sandstone. F1* denotes the mint green F1 near the basal contact

DISCUSSION

Our study aims to: 1) provide a local depositional history for the Mussentuchit Member, 2) reassess the basal contact of the Mussentuchit Member, 3) correlate fossil-bearing strata to key transgression and regression cycles found elsewhere in the Western Interior Seaway, and 4) provide novel stratigraphic linkages across the Western Interior Seaway. To date, no sedimentological evidence exists for apparent flooding by marine waters or back-building of the shore face; however, we establish a reasonable line of evidence for an altered regional base-level with a poorly drained subsurface in the landward portion of the paralic depocenter.

Paralic Reconstruction

As a whole, the Mussentuchit Member is described as weathered slopes of drab gray bentonitic muds and rare sandstones. Yet, on closer examination, the Mussentuchit Member preserves a broad suite of mud-rich sedimentary facies. With the reassignment of "Mussentuchit Member basal channel complex" (Garrison et al. 2007) to the uppermost Ruby Ranch, facies preserved in the Mussentuchit Member exemplify distal mud-dominated sedimentary successions (Fig. 11). The newly reassigned channel complex would be very similar to those described most recently by Cardenas et al. (2020), preserved in the exposed Ruby Ranch Member south of Green River, Utah. This depocenter would have been landward from the backshore and distal from the fluvial floodplain, removed from a major migrating channel belt. Herein, we do not present evidence for shoreface or nearshore facies; however, we do present evidence for the co-occurrence of distal fluvial and landward coastal plain sub-environments, defined as paralic (Reynolds 1999; Kjerfve et al. 2002; Reed et al. 2009; Tagliapietra et al. 2009; Colombera et al. 2016; Cavin 2017; Hampson et al. 2017). The reader should note that local variation is significant. In the southern Willow Springs and to the north in Walker Flat, we identified a greater frequency of muddy, distal alluvial processes, and greater frequency of organic-matter (OM) accumulation (wetlands), whereas in central and northern Willow Springs and the Mussentuchit Flat distal alluvial processes are infrequent. The inordinately high percentage of mud or clay fractions in nearly all facies, regardless of geographic or stratigraphic position, indicates this that depocenter sequestered muds and clays. Thereafter, emplaced sediments underwent either pedogenic or distal alluvial modification. Accumulation of OM can range from unidentifiable disseminated fragments to moderately preserved leaves, stems, root traces, and an isolated branch–trunk, indicating that floral assemblages range from parautochthonous to autochthonous. Invertebrate fossils are limited to a handful of oyster-like (molluscan) and bivalve-type shells in variable preservation states, and trace fossils are rare or poorly preserved.

The lower Mussentuchit Member, in the central and northern Willow Springs and most of the Mussentuchit Flat, is a series of stacked thin- to thick-bedded (1.0 cm to ± 2.5 m) volcaniclastic-rich muddy gleysols (F1) (Fig. 13). Based on the above information, we find it reasonable to interpret that this geographical area was affected by periodic water retention, followed by drainage. A relatively high base-level in subsurface sediments by resident groundwater (gleying) would likely have been mixed-water or brackish, a readily available source of abundant sulfate in marine-influenced deposition such as F1 (Ward 2002; Ludvigson et al. 2010, p. 15). Distinctively, this area lacks large-scale channelized architecture; rather, distal alluvial endmembers of infrequent broad-sweeping suspension-settling sheet floods (F3a) and variable extensive crevasse splays (F3b). The topography of this area seems to have been low-lying, with infrequent episodes of sediment input and long periods of pedogenic modification. Conversely, the southwestern part of Willow Springs and to the north in Walker Flat preserve a vastly different assemblage of facies. Although F1 gleysols are present, more commonly F6 coastal wetlands co-occur with distal sheet floods (F3a), splays (FA3b), dendritic channels (F3c), and muddy channel complexes (F7) indicate more active sediment alteration and emplacement nearer to an alluvial endmember, such as a river mouth or a delta plain. Therefore, this indicates that distal fluvial processes would push into a vast low-lying vegetated coastal wetland. Although both areas are markedly different, mud and clay-rich sediment emplacement in the lower Mussentuchit Member is herein interpreted to have occurred in the paralic zone between the fluvial floodplain to the west and coastal margin to the east (Reading 2009; James and Dalrymple 2010; Longhitano et al. 2012; Zakaria 2016).

Additional to the above sedimentological evidence, stable isotopes suggest that the average meteoric water from the Mussentuchit Member ranged between –5.8 to –6.2‰ VSMOW, based on pedogenic carbonate nodules, turtle phosphate (bone), and crocodile-tooth phosphate (Suarez et al. 2012) (Fig. 13). Even if turtle values are recalculated with the turtle–water equation of Coulson et al. (2008), the meteoric water from turtles is yet more depleted and averages –6.6‰VSMOW. These values are consistent with modeled meteoric water from latitudinal gradients as determined by pedogenic carbonate nodules from the equator to the pole (Suarez et al. 2011). The average Western Interior Seaway (WIS) value was likely depleted due to high-elevation freshwater input along the western margin of the WIS (Zhou et al. 2008; Suarez et al. 2011), and estimates for the WIS are as δ^{18}O-depleted as δ^{18}OWIS = –1.1‰ VSMOW. The most enriched meteoric-water values, calculated from turtles and mudstone micritic calcite cement, are –4.6‰ and –4.9‰, respectively. Using a median value of –4.8‰, a freshwater end-member median value of meteoric water of –6‰, and a simple mixing model with fully marine water, δ^{18}OWIS = –1.1‰, approximately 25% WIS seawater could cause the heavy end-member values observed in turtles and calcite. The heavier values calculated from turtles and crocodiles are from sites in the Mussentuchit Flat area (~ 16 m below the Naturita). This is consistent with the interpretation of a high base-level of brackish water from facies analysis of the lower part of the upper Mussentuchit Member.

The upper Mussentuchit Member is a coalescence of varied micro-depocenters in the evolving, more subaerial paralic depocenter (Fig. 13). Southern Willow Springs and to the north in Walker Flat preserve a series of more frequently occurring distal alluvial settings (splays, sheet floods, and levees) associated with distinct, but rare, multilateral fluvial channel sandstones. Transitions are the distinct shift from well-developed gleysols (F1) to histosols (F2) corresponding to an increased frequency of carbonaceous mudrocks, coal and coalified plant fragments, with the incursions of complex plant communities and a base-level fall. This was identified across the mapping area with increased frequency of identified ephemeral ponds, which accumulated decayed plant debris (OM) in low-lying topographic depressions lacking outlets (F4) rather than extensive wetlands. The increase in OM and peaty sediment is matched by the decrease in mottling with an increased frequency of slickensides. The only evidence for the accumulation of coarser wave and storm sediment lacking muds is F5, with the identification of non-shelly and shelly relict storm surge-driven gravel–sand ridges modified to dunes or pre-chenier ridges. Support for storm-surge emplacement also leans on the isolated oyster (molluscan bed). A single stratum of disarticulated to fractured oyster shell hash supported by sandy matrix, lacking escape structures, accumulated on the shore face to backshore and mobilized backward (redeposited) on the landward paralic zone (time-averaged-parautochthonous) during a storm surge. We interpret the uppermost Mussentuchit Member was deposited along a more subaerially exposed (landward) area of the coastal plains near encroaching distal-floodplain processes (fluvial) with ongoing base-level fall (Fig. 13).

The diversity of taxa preserved in the Mussentuchit Member, including mammal teeth, take into consideration the calculation of the relative humidity and aridity index (ε) (Levin et al. 2006). Overall humidity is consistent with ranges seen on modern coastal plains in the moist

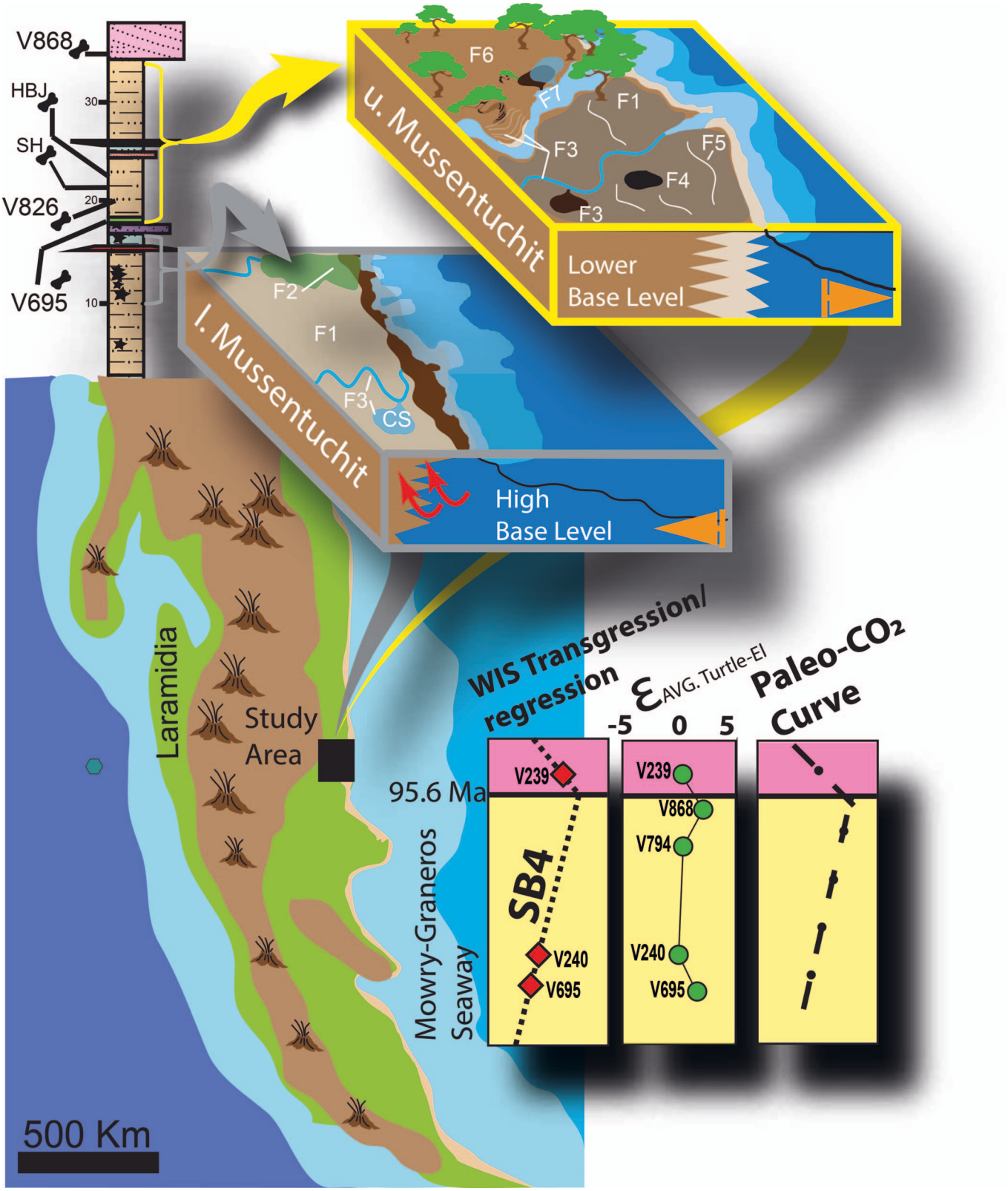

FIG. 13.—Facies reconstruction for the lower Mussentuchit Member with higher base-level, the upper Mussentuchit Member developing cheniers and co-occurring development of gleysols and histosols, channel complexes, and ephemeral pools with a relative fall in base-level and the nearshore coastal deposits of the Naturita. Transgression and regression data are based on Ohoh-Ikuenobe et al. (2008), Aridity Index Average of evaporite insensitive reptiles (turtle) modified from Suarez et al. (2012; Fig. 10), and decreases in CO_2 in the Cenomanian before the Cenomanian–Turonian Thermal Maximum as described by Wang et al. (2014), which resulted in a brief drop in sea level and a glacial episode for the upper Mussentuchit Member.

subtropical mid-latitude climatic regime (50–90% relative humidity) (Beck et al. 2005). Aridity index (ε) is calculated from the oxygen-isotope composition of phosphate between evaporation-sensitive taxa (terrestrial based organisms such as herbivores) and evaporation-insensitive taxa (aquatic-based taxa such as turtles and crocodiles). Positive and greater ε values represent increased aridity, whereas lower and negative ε values represent less aridity. In the case of the Mussentuchit Member, overall humidity is moderate to high and shifts in ε as described by Suarez et al. (2012) (Fig. 12) likely represent a shift in local environment from a proximal coastal setting to a more distal coastal or continental setting coupled with base-level fall. Lastly, facies-indicator taxa such as *Lonchidion* should be interpreted with caution as we find mounting evidence that this and other preserved taxa in the Mussentuchit Member were utilizing a paralic zone with mixed microecosystems influenced by mixed-water processes (Welton and Farish 1993; Noriega 1996; Bhattacharya and MacEachern 2009; Suarez et al. 2012, 2021; Kirkland et al. 2013).

Correlation of Transgressive–Regressive Cycles

Oboh-Ikuenobe et al. (2008) present biostratigraphic correlation and geochronologic ages, providing relatively well-constrained transgressive–regressive cycles for the WIS. They suggest that the Kiowa–Skull Creek transgression represents the first connection of Boreal and Tethyan waters at approximately 104 Ma. After the Kiowa–Skull Creek transgression, a minor regression, sequence boundary (S.B.) 1, split the WIS into a northern and southern arm. Another transgression occurred at ∼ 99–98 Ma with a transgression of 3.1; thereafter a minor regressive event (S.B. 3.2) occurred and is mostly expressed in the southern part of the WIS in Colorado and New Mexico. The Dry Creek–Pajarito transgression occurred at ∼ 98–97 Ma (transgression 3.2). It is again preserved best in southern Colorado and northern New Mexico. Another regression (S.B. 4) was preserved as a fluvial stratum of the Romeroville Sandstone. Finally, the Graneros transgression of the long-term Greenhorn cycle begins at approximately 97 Ma, culminating in a maximum-flooding surface preserved in the Thatcher Limestone of New Mexico at ∼ 95.4 Ma.

Tucker et al. (2020) employed CA-TIMS to demonstrate that the youngest subset of LA-ICP-MS-derived ages from detrital zircons in the Mussentuchit Flat were altered by lead loss and simultaneously identified that the youngest maximum depositional age (detrital zircon) of the basal Naturita was emplaced no later than 95.64 ± 0.11 Ma. Therefore, the upper Mussentuchit Member was likely emplaced up to 95.6 Ma. Suarez et al. (2012) used shifts in ε, humidity, and ^{39}Ar-^{40}Ar dates from Cifelli et al. (1997 1999), and transgressive–regressive cycles constrained by biostratigraphy and geochronology of Oboh-Ikuenobe et al. (2008) to suggest that two transgressive–regressive cycles of the Kiowa–Skull Creek to Greenhorn cycle of the Zuni Sequence are expressed in these changing humidity conditions. Based on the age constraints from Tucker et al. (2020) and recent fieldwork that reassess the stratigraphic location of the sites, only sites V695, V694, V235, V794, and V868 (see Fig. 2 of Suarez et al. 2012, and our Fig. 13) can be confirmed in the stratigraphic succession. Additionally, it is likely that all of the sites are within the defined upper Mussentuchit Member to lower Naturita (V293). As such, we suggest only the regressive cycle before the initiation of the Greenhorn cycle or the SB4 of Ohoh-Ikuenobe et al. (2008) is expressed in the increasing aridity index (ε) from sites 15 to 4 m below the Naturita Sandstone. Using this proxy, the lower Mussentuchit Member could be correlative to late TS 3.1; the more drained chenier plain of the upper Mussentuchit Member would be correlative to the regressive phase SB4 that occurs at ∼ 97–96 Ma, which roughly correlates to the Romeroville Sandstone, just before the start of the Greenhorn cyclothem. At a continental scale this would indicate that the Mussentuchit Member is near coeval with the paralic depocenters preserved in the Tuluvak Formation ("topset of the Seabee–Tuluvak depositional sequence") of Alaska (96.7 to 94.2 Ma; Shimer et al. 2016) uppermost Shaftesbury Formation to lower Dunvegan Formation of British Columbia–Alberta (± 95.8 Ma; Dufresne et al. 2001; Plint and Wadsworth 2003; Barker et al. 2011), and the Cenomanian Raritan facies of the upper Potomac Formation (Lipka et al. 1998; White et al. 2000; Gandolfo et al. 2001; Miller et al. 2004; Brownstein 2018). This would strengthen previous correlations of North American paralic coastal deposits suggested by White et al. (2000). Thereafter, the overlying Naturita Sandstone would be correlative to the transgressive phase and eventually Thatcher Limestone of the Greenhorn cycle, as mentioned above. This also fits well with recently published ages for the lower part of the middle Naturita of 95.98 ± 0.12 Ma from Laurin et al. (2019) with the Mussentuchit Member–Naturita Sandstone boundary still being time transgressive, but with a span of less than one million years (∼ 300,000 years) (Tibert et al. 2003; Laurin and Sageman 2007). At a broader scale, and based on recent age data, the Naturita Sandstone would also roughly correlate to the deltaic Woodbine Formation (∼ 95 Ma) of Texas (Main 2013)

CONCLUSIONS

1) Mussentuchit Member depositional setting: Detailed facies analysis and architectural reconstruction of sediment successions preserved in the Mussentuchit Member has enhanced our understanding of this particularly complex depocenter. Based on recovered data, we interpret that mud-rich sediments (sequestered muds and clays) were emplaced on a broad sweeping plain influenced by both distal alluvial (floodplain) and backshore (delta plain) processes. Major influences on sediment emplacement and subsequent local modification include a complex relationship between the updip migration of brackish groundwater into this depocenter coupled with pedogenic processes (like those described by White et al. 2005).

This was coeval with minor influences of distal tidal processes (bidirectional mud drapes on trough sets and wetlands), mixed-process deposits (wave-built gravel–sand ridges or washover fans modified to distal dunes and pre-chenier or shelly relict storm-surge-driven accumulations), and distal alluvial processes (sheet floods, splays, minor dendritic channels) all occurred just above the supratidal zone in this landward area of a paralic depocenter.

We identify a base-level rise of brackish groundwater in the lower Mussentuchit and subsequent fall in the upper Mussentuchit. Observations in the lower Mussentuchit include: 1) pyrite and other iron sulfide-based effluorescenses coupled with pervasive mottling, 2) evidence for vast, plant-rich wetlands (F2), 3) heavier δ^{18}O, and higher humidity levels. The transition to the upper Mussentuchit and an overall base-level fall is observed by: 1) a shift from mottling to pervasive slickensides coupled with the shift from gleysols to histosols, 2) more frequently occurring distal alluvial endmembers (channels and splays), 3) lighter δ^{18}O, and 4) great amounts of fluctuation in humidity levels. These particular sediment-based observations mirror facies and processes recently described in the Trinity Group, Holly Creek Formation by Suarez et al. (2021).

However, an obvious hindrance to our interpretation of the Mussentuchit Member as a paralic depocenter is the lack of pervasive bioturbation structures, typical of marine-influenced (tide or wave) paralic deposits. Our impoverished ichnofossil record may reflect a preservation bias or that the generation of traces in this landward area of the paralic depocenter was episodic not recurrent (Zennon and Dashtgard 2019). Alternatively, a lack of bioturbation structures may indicate ongoing stress or disturbances in ecosystems such as input of fine-grained sediment, higher levels of organic matter, or a reduced base-level and more input of fresh water into the ecosystem (Hassan et al. 2013; Hasiotis et al. 2013). We have a handful of identified traces ranging from simple *Skolithos* with secondary infill (typically clay) and a tentative "Y"-shaped *Thalassinoides* that support a

paralic setting. Herein, we interpret that the rarity of traces is likely a combination of the above-mentioned factors, and we must solidify our paleoenvironmental interpretation on key but subtle sedimentological data.

2) Reassessment of the basal contact of the Mussentuchit Member: We propose the following criteria for the stratigraphy of the Mussentuchit Member as opposed to Garrison et al. (2007): 1) *If the Short Canyon is absent and the Ruby Ranch channel sandstone is present*, the contact should be ± 2.0 m above a resistant, ± 1.0 m thick, trough cross-bedded channel sandstone coupled with the last occurrence of pervasive carbonate nodule drapes and the first occurrence of bentonitic mint green and gray mudrocks; and 2) *if the Short Canyon is present*, the contact should be observed with the last occurrence of a pebble-lag drape or a bedded oligomictic paracongomerate coupled with the first occurrence of bentonitic mint green and gray mudrocks.

3) Correlation of transgression and regression cycles in the Western Interior Seaway: We draw special attention to the shift in landscape evolution preserved in the Mussentuchit Member to the above-mentioned altered regional base level. Due to this line of evidence, coupled with age dates presented in Tucker et al. (2020), we interpret that the lower Mussentuchit Member correlates to the late stages of TS 3.1 resulting in the updip migration of brackish groundwater, immediately followed by the S.B. 4 Regression of the Western Interior Seaway (Greenhorn cycle) and the downdip migration of brackish groundwaters. At a broader scale our middle to later Cenomanian TS 3.1 to S.B. 4 regression would directly correlate with drops in overall global sea-level fall in response to a mid- to late Cenomanian brief glacial phase (drop in paleo-CO_2) before the Cenomanian–Turonian Thermal Maximum (Wang et al. 2014).

4) Provide novel stratigraphic linkages: In a Western Interior context, based on the S.B. 4 identification and age dates presented in Tucker et al. (2020), we correlate the Mussentuchit Member to the deltaic Romeroville Sandstone of New Mexico and the Woodbine Formation of Texas. At a broader scale and based on the earlier work of White et al. (2000), we can formulate novel linkages for the Mussentuchit Member to other near-contemporaneous paralic depocenters, including: 1) the Tuluvak Formation (“topset of the Seabee–Tuluvak depositional sequence”) of Alaska, 2) uppermost Shaftesbury Formation to lower Dunvegan Formation of British Columbia–Alberta, and 3) the Cenomanian Raritan facies of the upper Potomac Formation of New Jersey.

With these findings we further support the supposition that the Cedar Mountain Formation, and especially the Mussentuchit Member, was a transitional ecosystem, from floodplain alluvial deposits in the underlying Brushy Basin Member of the Morrison Formation to the foreshore and shoreface deposits in the overlying Naturita Sandstone (Eberth et al. 2006; Chure et al. 2010). Furthermore, based on these accumulating observations, we interpret that the Mussentuchit Member locally was an evolving coastal plain (paralic depocenter), similar to the current coastal plains of French Guiana (Augustinus 1989; Prost 1989; Healy et al. 2002; I-Iealy et al. 2002; Wang et al. 2002; Proisy et al. 2009; Fan et al. 2012).

ACKNOWLEDGMENTS

We thank staff, students, and volunteers of the 2015–2019 expeditions for repeated explorations of the Mussentuchit Member: M. Leschin, S. Foss, G. McDonald, R. Anderson, R. Hunt-Foster, J. Kirkland, M. Hayden, J. Krishna, R. Irmis. The staff of the Price Field Office, the Bureau of Land Management, Utah State Office, the Natural History Museum of Utah, and the Utah Geological Survey are thsnked for permitting and expedition support. Financial support was provided by Stellenbosch University’s Department of Earth Sciences, North Carolina Museum of Natural Sciences, the Canyonlands Natural History Association, Field Museum of Natural History, the DRD, and National Science Foundation awards FRES 1925884, 1925973, and 1925915. Any opinions, findings, and conclusions or recommendations expressed in this material are those of the authors and do not necessarily reflect the views of the National Science Foundation. Finally, we wish to thank editor K.M. Marsaglia, the generous reviewers W.W. Little and P. Flaig, associate editor G. Ludvigson, and corresponding editor J.B. Southard, along with anonymous persons for their feedback and improvements to this manuscript.

REFERENCES

Al-Suwaidi, A.H., 2007, A Ped’s Story: Weathering out Climatic Change during the mid-Cretaceous [M.S. Thesis]: University of Kansas, 134 p.

Anthony, E.J., Gardel, A., Gratiot, N., Proisy, C., Allison, M.A., Dolique, F., and Fromard, F., 2010, The Amazon-influenced muddy coast of South America: a review of mud-bank–shoreline interactions: Earth-Science Reviews, v. 103, p. 99–121.

Anthony, E.J., Gardel, A., and Gratiot, N., 2014, Fluvial sediment supply, mud banks, cheniers and the morphodynamics of the coast of South America between the Amazon and Orinoco river mouths: Geological Society of London, Special Publication 388, p. 533–560.

Augustinus, P., 1989, Cheniers and chenier plains: a general introduction: Marine Geology, v. 90, p. 219–229.

Avrahami, H.M., Makovicky, P.J., and Zanno, L.E., 2019, Paleohistology of a new Orodromine from the Upper Cretaceous (Cenomanian) Mussentuchit Member of the Cedar Mountain Formation, Utah: histological implications for burrowing behavior [Abstract]: Journal of Vertebrate Paleontology, Program Abstracts, v. 56.

Bann, K.L., Fielding, C.R., MacEachern, J.A., and Tye, S.C., 2004, Differentiation of estuarine and offshore marine deposits using integrated ichnology and sedimentology: Permian Pebbley Beach Formation, Sydney Basin, Australia, *in* McIlroy, D., ed., The Application of Ichnology to Paleoenvironmental and Stratigraphic Analysis: Geological Society of London, Special Publication 228, p. 179–211.

Barker, I.R., Moser, D.E., Kamo, S.L., and Plint, A.G., 2011, High-precision U-Pb zircon ID-TIMS dating of two regionally extensive bentonites: Cenomanian Stage, Western Canada Foreland Basin: Canadian Journal of Earth Sciences, v. 48, p. 543–556.

Bassett, D., MacLeod, K.G., Miller, J.F., and Ethington, R.L., 2007, Oxygen isotopic composition of biogenic phosphate and the temperature of Early Ordovician Seawater: Palaios, v. 22, p. 98–103.

Beck, C., Grieser, J., Kottek, M., Rubel, F., and Rudolf, B., 2005, Characterizing global climate change by means of Köppen climate classification: Klimastatusbericht, v. 51, p. 139–149.

Bhattacharya, J.P., and MacEachern, J.A., 2009, Hyperpycnal rivers and prodeltaic shelves in the Cretaceous seaway of North America: Journal of Sedimentary Research, v. 79, p. 184–209.

Bonde, J.W., Varricchio, D.J., Jackson, F.D., Loope, D.B., and Shirk, A.M., 2008, Dinosaurs and dunes! Sedimentology and paleontology of the Mesozoic in the Valley of Fire State Park: Geological Society of America, Field Guide 11, p. 249–262.

Brewer, R., and Sleeman, J.R., 1964, Glaebules: their definition, classification and interpretation: Journal of Soil Science, v. 15, p. 66–78.

Botfalvai, G., Haas, J., Bodor, E.R., Mindszenty, A., and Ősi, A., 2016, Facies architecture and palaeoenvironmental implications of the Upper Cretaceous (Santonian) Csehbánya Formation at the Iharkút vertebrate locality (Bakony Mountains, Northwestern Hungary): Palaeogeography, Palaeoclimatology, Palaeoecology, v. 441, p. 659–678.

Brown, C.M., Evans, D.C., Campione, N.E., O’Brien, L.J., and Eberth, D.A., 2013, Evidence for taphonomic size bias in the Dinosaur Park Formation (Campanian, Alberta), a model Mesozoic terrestrial alluvial-paralic system: Palaeogeography, Palaeoclimatology, Palaeoecology, v. 372, p. 108–122.

Brownstein, C.D., 2018, The biogeography and ecology of the Cretaceous non-avian dinosaurs of Appalachia: Palaeontologia Electronica, v. 21, p. 1–56.

Cardenas, B.T., Mohrig, D., Goudge, T.A., Hughes, C.M., Levy, J.S., Swanson, T., Mason, J., and Zhao, F., 2020, The anatomy of exhumed river-channel belts: bedform to belt-scale river kinematics of the Ruby Ranch Member, Cretaceous Cedar Mountain Formation, Utah, USA: Sedimentology, 67, p. 3655–3682.

Carpenter, K., 2014, Where the sea meets the land: the unresolved Dakota problem in Utah: Utah Geological Association, Publication 43, p. 357–372.

Chure, D., Britt, B.B., Whitlock, J.A., and Wilson, J.A., 2010, First complete sauropod dinosaur skull from the Cretaceous of the Americas and the evolution of sauropod dentition: Naturwissenschaften, v. 97, p. 379–391.

Cifelli, R.L., Kirkland, J.I., Weil, A., Deino, A.L., and Kowallis, B.J., 1997, High-precision $^{40}Ar/^{39}Ar$ geochronology and the advent of North America’s Late Cretaceous terrestrial fauna: National Academy of Sciences (USA), Proceedings, v. 94, p. 11163–11167.

Cifelli, R.L., Nydam, R.L., Gardner, J.D., Weil, A., Eaton, J.G., Kirkland, J.I., Madsen, S.K., and Gillette, D.D., 1999, Medial Cretaceous vertebrates from the Cedar Mountain Formation, Emery County, Utah: the Mussentuchit local fauna: Vertebrate Paleontology in Utah, v. 99, p. 219–242.

Cifelli, R.L., Nydam, R.L., Gardner, J.D., Weil, A., Eaton, J.G., Kirkland, J.I., Madsen, S.K., and Cavin, L., 2017, Freshwater environments and fishes, *in* Cavin, L., Freshwater Fishes: 250 Million Years of Evolutionary History: London, Elsevier, p. 1–11.

Choi, K., and Kim, S.P., 2006, Late Quaternary evolution of macrotidal Kimpo tidal flat, Kyonggi Bay, west coast of Korea: Marine Geology, v. 232, p. 17–34.

Cilliers, C.D., Tucker, R.T., Crowley, J.L., and Zanno, L.E., 2021, Age constraint for the Moreno Hill Formation (Zuni Basin) by CA-TIMS and LA-ICP-MS detrital zircon geochronology: PeerJ, 9:e10948

Colombera, L., Mountney, N.P., Hodgson, D.M., and McCaffrey, W.D., 2016, The shallow-marine architecture knowledge store: a database for the characterization of shallow-marine and paralic depositional systems: Marine and Petroleum Geology, v. 75, p. 83–99.

Coulson, A.B., Kohn, M.J., Shirley, M.H., Joyce, W.G., and Barrick, R.E., 2008, Phosphate-oxygen isotopes from marine turtle bones: ecologic and paleoclimatic applications: Palaeogeography, Palaeoclimatology, Palaeoecology, v. 264, p. 78–84.

Cross, T.A., and Pilger, R.H., 1978, Tectonic controls of Late Cretaceous sedimentation, western interior, USA: Nature, v. 274(5672), p. 653–657.

Currie, B.S., 1997, Sequence stratigraphy of nonmarine Jurassic–Cretaceous rocks, central Cordilleran foreland-basin system: Geological Society of America, Bulletin, v. 109, p. 1206–1222.

Currie, B.S., 2002, Structural configuration of the Early Cretaceous Cordilleran foreland-basin system and Sevier thrust belt, Utah and Colorado: The Journal of Geology, v. 110, p. 697–718.

Dalrymple, R.W., Baker, E.K., Harris, P.T., and Hughes, M.G., 2003, Tropical deltas of southeast Asia: sedimentology, stratigraphy, and petroleum geology, *in* Sidi, F.H., Nummedal, D., Imbert, P., Darman, H., and Posamentier, H.W., eds., Sedimentology and Stratigraphy of a Tide-Dominated Foreland-Basin Delta (Fly River, Papua New Guinea): SEPM, Special Publication 76, p. 147–173.

DeCelles, P.G., and Currie, B.S., 1996, Long-term sediment accumulation in the Middle Jurassic–early Eocene Cordilleran retroarc foreland-basin system: Geology, v. 4, p. 591–594.

DeCelles, P.G., and Graham, S.A., 2015, Cyclical processes in the North American Cordilleran orogenic system: Geology, v. 43, p. 499–502.

DeCelles, P.G., Lawton, T.F., and Mitra, G., 1995, Thrust timing, growth of structural culminations, and synorogenic sedimentation in the type Sevier orogenic belt, western United States: Geology, v. 23, p. 699–702.

D'Emic, M.D., Foreman, B., Jud, N.A., Britt, B.B., Schmitz, M., and Crowley, J.L., 2019, Chronostratigraphic revision of the Cloverly Formation (Lower Cretaceous, Western Interior, USA): Peabody Museum of Natural History, Bulletin, v. 60, p. 3–40.

Doelling, H.H., and Kuehne, P.A., 2013, Geologic map of the Short Canyon Quadrangle, Emery County, Utah: Utah Geological Survey, Map 255DM, 31 p., 2 plates, scale 1:24,000.

Driebergen, J., Cifelli, R., Zanno, L.E., and Makovicky, P.J., 2017, Comparative taphonomy of two juveniles *Eolambia caroljonesa* (Hadrosauria) bonebeds from the Cedar Mountain Formation of Utah [Abstract]: Journal of Vertebrate Paleontology, Program Abstracts, v. 105.

Dufresne, M.B., Eccles, D.R., and Leckie, D.A., 2001, Geological and geochemical setting of the mid-Cretaceous Shaftesbury Formation and other Colorado Group sedimentary units: Alberta Energy and Utilities Board, Alberta Geological Survey, Special Report 9.

Eaton, J.G., Kirkland, J.I., and Kauffman, E.G., 1990, Evidence and dating of mid-Cretaceous tectonic activity in the San Rafael Swell, Emery County, Utah: The Mountain Geologist, v. 27, p. 39–45.

Eberth, D.A., and Miall, A.D., 1991, Stratigraphy, sedimentology and evolution of a vertebrate-bearing, braided to anastomosed fluvial system, Cutler Formation (Permian–Pennsylvanian), north-central New Mexico: Sedimentary Geology, v. 72, p. 225–252.

Eberth, D.A., Britt, B.B., Scheetz, R., Stadtman, K.L., and Brinkman, D.B., 2006, Dalton Wells: geology and significance of debris-flow-hosted dinosaur bonebeds in the Cedar Mountain Formation (Lower Cretaceous) of eastern Utah, USA: Palaeogeography, Palaeoclimatology, Palaeoecology, v. 236, p. 217–245.

Eswaran, H., and Reich, P.F., 2005, World Soil Map: Encyclopedia of Soils in the Environment, p. 352–365, doi:10.1016/b0-12-348530-4/00019-9.

Fan, D., 2012, Open-coast tidal flats, *in* Davis, R.A., and Dalrymple, R.W., eds., Principles of Tidal Sedimentology: Dordrecht, Springer, p. 187–229.

Fan, D., Yuan, W., and Min, L., 2013, Classifications, sedimentary features and facies associations of tidal flats: Journal of Palaeogeography, v. 2, p. 66–80.

Farke, A.A., Maxwell, W.D., Cifelli, R.L., and Wedel, M.J., 2014, A Ceratopsian Dinosaur from the Lower Cretaceous of western North America, and the biogeography of Neoceratopsia: PLOS One, e112055, doi:10.1371/journal.pone.0112055.

Finkl, C.W., 2019, Beach ridges: Encyclopedia of Earth Sciences Series: Encyclopedia of Coastal Science, p. 290–296.

Frederickson, J.A., Cohen, J.E., Hunt, T.C., and Cifelli, R.L., 2017, A new occurrence of *Dakotasuchus kingi* from the Late Cretaceous of Utah, USA, and the diagnostic utility of postcranial characters in Crocodyliformes: Acta Palaeontologica Polonica, v. 62, p. 279–286.

Frederickson, J.A., Engel, M.H., and Cifelli, R.L., 2018, Niche partitioning in Theropod Dinosaurs: diet and habitat preference in predators from the Uppermost Cedar Mountain Formation (Utah, USA): Scientific Reports, v. 8, p. 1–13.

Frucci, M.N., 2018, Oxygen isotopic composition of aquatic reptile phosphate from the Early Cretaceous Holly Creek Formation, southern Arkansas [B.S. Honors Thesis]: University of Arkansas, 22 p.

Gale, A.S., Hardenbol, J., Hathway, B., Kennedy, W.J., Young, J.R., and Phansalkar, V., 2002, Global correlation of Cenomanian (Upper Cretaceous) sequences: evidence for Milankovitch control on sea level: Geology, v. 30, p. 291–294.

Galli, G., 1991, Mangrove-generated structures and depositional model of the Pleistocene Fort Thompson Formation (Florida Plateau): Facies, v. 25, p. 297–314.

Gandolfo, M.A., Nixon, K.C., and Crepet, W.L., 2001, Turonian Pinaceae of the Raritan Formation, New Jersey: Plant Systematics and Evolution, v. 226, p. 187–203.

Garrison, J.R., Jr., Brinkman, D., Nichols, D.J., Layer, P., Burge, D., and Thayn, D., 2007, A multidisciplinary study of the Lower Cretaceous Cedar Mountain Formation, Mussentuchit Flat, Utah: a determination of the paleoenvironment and paleoecology of the *Eolambia caroljonesa* dinosaur quarry: Cretaceous Research, v. 28, p. 461–494.

Giallorenzo, M.A., Wells, M.L., Yonkee, W.A., Stockli, D.F., and Wernicke, B.P., 2018, Timing of exhumation, Wheeler Pass thrust sheet, southern Nevada and California: Late Jurassic to middle Cretaceous evolution of the southern Sevier fold-and-thrust belt: Geological Society of America, Bulletin, v. 130, p. 558–579, doi:10.1130/B31777.1.

Gill, A.M., and Tomlinson, P.B., 1977, Studies on the growth of red mangrove (*Rhizophora mangle L.*): the adult root system: Biotropica, p. 145–155.

Gillette, D.D., 1999, Medial Cretaceous vertebrates from the Cedar Mountain Formation, Emery County, Utah: the Mussentuchit local fauna: Vertebrate Paleontology in Utah, v. 99, p. 219–242.

Gingras, M.K., MacEachern, J.A., and Dashtgard, S.E., 2012, Estuaries, *in* Knaust, D., and Bromly, R.G., eds., Trace Fossils as Indicators of Sedimentary Environments: Elsevier, Developments in Sedimentology, v. 64, p. 471–514.

Goddard, E.N., Trask, P.D., De Ford, R.K., Rove, O.N., Singewald, J.T., Jr., and Overbeck, R.M., 1995, America Rock Color Chart: Geological Society of America.

Goldberg, P., 2000, Faunal associations and compositional differences among sites in the Mussentuchit Member of the Cedar Mountain Formation [Ph.D. Thesis]: University of Oklahoma, 206 p.

Greenhalgh, B.W., and Britt, B.B., 2007, Stratigraphy and sedimentology of the Morrison–Cedar Mountain Formation boundary, east-central Utah, *in* Willis, G.C., Hylland, M.D., Clark, D.L., and Chidsey, T.C., Jr., eds., Central Utah: Diverse Geology of a Dynamic Landscape: Utah Geological Association, Publication 36, p. 81–100.

Hampson, G.J., Reynolds, A.D., Kostic, B., and Wells, M.R., 2017, Introduction to the sedimentology of paralic reservoirs: recent advances: Geological Society of London, Special Publication 444, p. 1–6.

Harris, D.R., 1980, Exhumed paleochannels in the Lower Cretaceous Cedar Mountain Formation near Green River, Utah [Ph.D. Thesis]: Brigham Young University, Geological Studies, v. 27, p. 51–66.

Hasiotis, S.T., McPherson, J.G., and Reilly, M.R.W., 2013, Using ichnofossils to reconstruct the depositional history of sedimentary successions in alluvial, coastal-plain, and deltaic settings: European Association of Geoscientists and Engineers, International Petroleum Technology Conference, p. 350.

Hassan, M.H.A., Johnson, H.D., Allison, P.A., and Abdullah, W.H., 2013, Sedimentology and stratigraphic development of the upper Nyalau Formation (Early Miocene), Sarawak, Malaysia: a mixed wave-and tide-influenced coastal system: Journal of Asian Earth Sciences, v. 76, p. 301–311.

Healy, T., Wang, Y., and Healy, J.A., 2002, Definition, properties, and classification of muddy coasts, *in* Healy, T., Wang, Y., and Healy, J.A., eds., Muddy Coasts of the World: Processes, Deposits and Function: Elsevier, Proceedings in Marine Science 4, p. 9.

Hintze, L.F., Willis, G.C., Laes, D.Y., Sprinkel, D.A., and Brown, K.D., 2000, Digital geologic map of Utah: 179DM, scale 1:500,000.

Hong, S.H., Chang, T.S., Lee, G.S., Kim, J.C., Choi, J., and Yoo, D.G., 2019, Late Pleistocene–Holocene sedimentary facies and evolution of the Jeju Strait shelf, southwest Korea: Quaternary International, v. 519, p. 156–169.

Hunt, G.J., Lawton, T.F., Kirkland, J.I., Sprinkel, D.A., Yonkee, W.A., and Chidsey, T.C., 2011, Detrital zircon U-Pb geochronological provenance of Lower Cretaceous strata, foreland basin, Utah, in Sprinkel, D.A., ed., Sevier Thrust Belt: Northern and Central Utah and Adjacent Areas: Utah Geological Association, v. 40, p. 193–211.

I-Iealy, T., Wang, Y., and Healy, J.A., 2002, Geographic distribution of muddy coasts, *in* Healy, T., Wang, Y., and Healy, J.A., eds., Muddy Coasts of the World: Processes, Deposits and Function: Elsevier, Proceedings in Marine Science 4, p. 99–201.

Ielpi, A., 2013, Frequency-reliant correlative patterns of asymmetric lacustrine–paralic sequences: a genetic approach to the late Miocene Bithynia marlstones of the southeastern Volterra Basin, Italy: Journal of Sedimentary Research, v. 83, p. 377–394.

James, N.P., and Dalrymple, R.W., 2010, Facies Models 4: Geological Association of Canada, 586 p.

Jinnah, Z.A., and Roberts, E.M., 2011, Facies associations, paleoenvironment, and base-level changes in the Upper Cretaceous Wahweap Formation, Utah, USA: Journal of Sedimentary Research, v. 81, p. 266–283.

Johnson, P.N., and Rogers, G.M., 2003, Ephemeral wetlands and their turfs in New Zealand: Science for Conservation, v. 230, p. 1–109.

Kamola, D.L., 1984, Trace fossils from marginal-marine facies of the Spring Canyon Member, Blackhawk Formation (Upper Cretaceous), east-central Utah: Journal of Paleontology, p. 529–541.

Kauffman, E.G., 1984, Paleobiogeography and evolutionary response dynamic in the Cretaceous Western Interior Seaway of North America, *in* Westermann, G.E.G., ed., Jurassic–Cretaceous Biochronology and Paleogeography of North America: Geological Association of Canada, Special Paper 27, p. 273–306.

Kaya, M.Y., Dupont-Nivet, G., Proust, J.N., Roperch, P., Meijer, N., Frieling, J., Fioroni, C., Özkan Altiner, S., Stoica, M., Aminov, J., and Mamtimin, M., 2020, Cretaceous evolution of the Central Asian proto-Paratethys Sea: tectonic, eustatic, and climatic controls: Tectonics, v. 39, p. 1–27.

Kirkland, J.I., 1998, A new hadrosaurid from the upper Cedar Mountain Formation (Albian–Cenomanian: Cretaceous) of eastern Utah: the oldest known hadrosaurid

(lambeosaurine?), *in* Lucas, S.G., Kirkland, J.I., and Estep, J.W., eds., Lower and Middle Cretaceous Terrestrial Ecosystems: New Mexico Museum of Natural History and Science, Bulletin 14, p. 283–295.

Kirkland, J.I., and Madsen, S.K., 2007, The Lower Cretaceous Cedar Mountain Formation eastern Utah: the view up an always interesting learning curve, *in* Lund, W.L., ed., Field Guide to Geological Excursions in Southern Utah: Geological Society of America, p. 1–108, CD-ROM.

Kirkland, J.I., Cifelli, R.L., Britt, B.B., Burge, D.L., DeCourten, F.L., Eaton, J.G., Parrish, J.M., and Gillette, D.D., 1999, Distribution of vertebrate faunas in the Cedar Mountain Formation, east-central Utah: Vertebrate Paleontology in Utah, v. 99, p. 201–218.

Kirkland, J.I., Eaton, J.G., and Brinkman, D.B., 2013, Elasmobranchs from Upper Cretaceous freshwater facies in southern Utah: at the top of the Grand Staircase, *in* Loewen, A., and Titus, M., eds., The Late Cretaceous of Southern Utah: Indiana University Press, Bloomington, p. 153–194.

Kirkland, J.I., Suarez, M., Suarez, C., and Hunt-Foster, R., 2016, The Lower Cretaceous in east-central Utah: the Cedar Mountain Formation and its bounding strata: Geology of the Intermountain West, v. 3, p. 101–228.

Kirschbaum, M.A., and Schenk, C.J., 2010, Sedimentology and reservoir heterogeneity of a valley-fill deposit: a field guide to the Dakota Sandstone of the San Rafael Swell, Utah: U.S. Geological Survey, Scientific Investigations, Report 2010-5222, 36 p.

Kjerfve, B., Perillo, G.M., Gardner, L.R., Rine, J.M., Dias, G.T., and Mochel, F.R., 2002, Morphodynamics of muddy environments along the Atlantic coasts of North and South America, *in* Healy, T., Wang, Y., and Healy, J.A., eds., Muddy Coasts of the World: Processes, Deposits and Function: Elsevier, Proceedings in Marine Science 4, p. 479–532.

Knaust, D., and Bromley, R.G., eds., 2012, Trace Fossils as Indicators of Sedimentary Environments: Amsterdam, Elsevier, 924 p.

Kohn, M.J., 1996, Predicting animal $\delta^{18}O$: accounting for diet and physiological adaptation: Geochimica et Cosmochimica Acta, v. 60, p. 4811–4829.

Laurin, J., and Sageman, B.B., 2007, Cenomanian–Turonian coastal record in SW Utah, USA: orbital-scale transgressive–regressive events during Oceanic Anoxic Event II: Journal of Sedimentary Research, v. 77, p. 731–756.

Laurin, J., Barclay, R.S., Sageman, B.B., Dawson, R.R., Pagani, M., Schmitz, M., Eaton, J., McInerney, F.A., and McElwain, J.C., 2019, Terrestrial and marginal-marine record of the mid-Cretaceous Oceanic Anoxic Event 2 (OAE 2): high-resolution framework, carbon isotopes, CO_2, and sea-level change: Palaeogeography, Palaeoclimatology, Palaeoecology, v. 524, p. 118–136.

Levin, N.E., Cerling, T.E., Passey, B.H., Harris, J.M., and Ehleringer, J.R., 2006, A stable isotope aridity index for terrestrial environments: National Academy of Sciences (USA), Proceedings, v. 103, p. 11201–11205.

Li, Y., Shao, L., Fielding, C.R., Wang, D., Mu, G., and Luo, H., 2020, Sequence stratigraphic analysis of thick coal seams in paralic environments: a case study from the Early Permian Shanxi Formation in the Anhe coalfield, Henan Province, North China: International Journal of Coal Geology, v. 222, p. 103451.

Lin, W., and Bhattacharya, J.P., 2020, Depositional facies and the sequence stratigraphic control of a mixed-process influenced clastic wedge in the Cretaceous Western Interior Seaway: the Gallup System, New Mexico, USA: Sedimentology, v. 67, p. 920–950.

Lin, W., Ferron, C., Karner, S., and Bhattacharya, J.P., 2020, Classification of paralic channel sub-environments in an ancient system using outcrops: the Cretaceous Gallup system, New Mexico, USA: Journal of Sedimentary Research, v. 90, p. 1094–1113.

Lin, W., Bhattacharya, J.P., Jicha, B.R., Singer, B.S., and Matthews, W., 2021, Has Earth ever been ice-free? Implications for glacio-eustasy in the Cretaceous greenhouse age using high-resolution sequence stratigraphy: Geological Society of America, Bulletin, v. 133, p. 243–252.

Lipka, T.R., 1998, The affinities of the enigmatic theropods of the Arundel Clay facies (Aptian), Potomac Formation, Atlantic coastal plain of Maryland, *in* Lucas, S.G., Kirkland, J.I., and Estep, J.W., eds., Lower and Middle Cretaceous Terrestrial Ecosystems: New Mexico Museum of Natural History and Science, Bulletin, v. 14, p. 229–234.

Liu, J., Cao, D., Zhang, Y., and Li, Y., 2020, Temporal changes in an epeiric paralic deposition during a third-order relative sea-level cycle (Late Pennsylvanian, western North China): insights from integrated facies and sequence stratigraphic analysis. Journal of Asian Earth Sciences, v. 196, p. 104349.

Longhitano, S.G., Mellere, D., Steel, R.J., and Ainsworth, R.B., 2012, Tidal depositional systems in the rock record: a review and new insights: Sedimentary Geology, v. 279, p. 2–22.

Lowery, C.M., Leckie, R.M., Bryant, R., Elderbak, K., Parker, A., Polyak, D.E., Schmidt, M., Snoeyenbos-West, O., and Sterzinar, E., 2018, The Late Cretaceous Western Interior Seaway as a model for oxygenation change in epicontinental restricted basins: Earth-Science Reviews, v. 177, p. 545–564.

Ludvigson, G.A., Joeckel, R.M., González, L.A., Gulbranson, E.L., Rasbury, E.T., Hunt, G.J., Kirkland, J.I., and Madsen, S., 2010, Correlation of Aptian–Albian carbon isotope excursions in continental strata of the Cretaceous foreland basin, eastern Utah, USA: Journal of Sedimentary Research, v. 80, p. 955–974.

MacEachern, J.A., Bann, K.L., Gingras, M.K., Zonneveld, J.P., Dashtgard, S.E., Pemberton, S.G., Knaust, D., and Bromley, R.G., 2012, Trace fossils as indicators of sedimentary environments: Developments in Sedimentology, v. 64, p. 103–138.

Mack, G.H., James, W.C., and Monger, H.C., 1993, Classification of paleosols: Geological Society of America, Bulletin, v. 105, p. 129–136.

Main, D.J., 2013, Appalachian delta plain paleoecology of the Cretaceous Woodbine Formation at the Arlington Archosaur Site, North Texas [Ph.D. Thesis]: University of Texas at Arlington, 548 p.

Makovicky, P.J., Shinya, A., and Zanno, L.E., 2014, New additions to the diversity of the Mussentuchit Member, Cedar Mountain Formation, Dinosaur fauna [Abstract]: Journal of Vertebrate Paleontology, Program Abstracts, p. 175.

Makovicky, P.J., Zanno, L.E., and Gates, T.A., 2015, The advent of North America's Late Cretaceous fauna revisited: insights from new discoveries and improved phylogenies [Abstract]: Journal of Vertebrate Paleontology, Program and Abstracts, p. 172–173.

Mannion, P.D., and Upchurch, P., 2011, A re-evaluation of the "mid-Cretaceous sauropod hiatus" and the impact of uneven sampling of the fossil record on patterns of regional dinosaur extinction: Palaeogeography, Palaeoclimatology, Palaeoecology, v. 299, p. 529–540.

Mannion, P.D., Benson, R.B., and Butler, R.J., 2013, Vertebrate palaeobiodiversity patterns and the impact of sampling bias: Palaeogeography, Palaeoclimatology, Palaeoecology, v. 372, p. 1–4.

McCabe, P.J., 1987, Facies studies of coal and coal-bearing strata, *in* McCabe, P.J., ed., Coal and Coal-Bearing Strata: Recent Advances: Geological Society of London, Special Publication 32, p. 51–66.

McDonald, A.T., Bird, J., Kirkland, J.I., and Dodson, P., 2012, Osteology of the basal Hadrosauroid *Eolambia caroljonesa* (Dinosauria: Ornithopoda) from the Cedar Mountain Formation of Utah: PLoS ONE, v. 7, p. e45712.

McDonald, A.T., Gates, T.A., Zanno, L.E., and Makovicky, P.J., 2017, Anatomy, taphonomy, and phylogenetic implications of a new specimen of *Eolambia caroljonesa* (Dinosauria: Ornithopoda) from the Cedar Mountain Formation, Utah, USA: PLoS ONE, v. 12, p. 0176896.

McIlroy, D., Flint, S., Howell, J.A., and Timms, N., 2005, Sedimentology of the tide-dominated Jurassic Lajas Formation, Neuquén Basin, Argentina: Geological Society of London, Special Publication 252, p. 83–107.

Miall, A.D., 1985, Architectural-element analysis: a new method of facies analysis applied to fluvial deposits: Earth-Science Reviews, v. 22, p. 261–308.

Miall, A.D., 2010, Alluvial deposits, *in* James, N.P., and Dalrymple, R.W., eds., Facies models 4: Geological Association of Canada, p. 105–137.

Miall, A.D., 2022, Facies analysis, *in* Miall, A.D., ed., Stratigraphy: A Modern Synthesis: Springer, p. 91–174.

Miller, K.G., Sugarman, P.J., Browning, J.V., Kominz, M.A., Olsson, R.K., Feigenson, M.D., and Hernández, J.C., 2004, Upper Cretaceous sequences and sea-level history, New Jersey coastal plain: Geological Society of America, Bulletin, v. 116, p. 368–393.

Miller, R.A., and Sigleo, W.R., 1984, Parameters related to the identification of paleosols in the geologic record: U.S. Geological Survey, Open-File Report, no. 83-776.

Morales, J.A., Borrego, J., and Davis, R.A., Jr., 2014, A new mechanism for chenier development and a facies model of the Saltés Island chenier plain (SW Spain): Geomorphology, v. 204, p. 265–276.

Munsell Color, 2009, Geological Rock Color Chart: Munsell Color, Grand Rapids.

Munsell Color, 2011, Geological Rock Color Chart: with Genuine Munsell Color Chips: Munsell Color.

Nelson, M.E., and Crooks, D.M., 1987, Stratigraphy and paleontology of the Cedar Mountain Formation (Lower Cretaceous), eastern Emery County, Utah, *in* Averett, W.R., Goodknight, C.S., Chenoweth, W.L., Ertel, D.B., Girdley, W.A., Hamblin, A.H., Dayvault, R.D., and Young, R.G., eds., Paleontology and Geology of the Dinosaur Triangle: American Association of Petroleum Geologists, Fieldtrip Guidebook, p. 55–63.

Nesbitt, S.J., Denton, R.K., Loewen, M.A., Brusatte, S.L., Smith, N.D., Turner, A.H., Kirkland, J.I., McDonald, A.T., and Wolfe, D.G., 2019, A mid-Cretaceous tyrannosauroid and the origin of North American end-Cretaceous dinosaur assemblages: Nature Ecology and Evolution, v. 3, p. 892.

Noriega, F.J.G., 1996, Cintura Formation: an Early Cretaceous deltaic system in northeastern Sonora, Mexico: Revista Mexicana de Ciencias Geológicas, v. 13, p. 129–139.

Oboh-Ikuenobe, F., Holbrook, J.M., Scott, R.W., Akins, S.L., Evetts, M.J., Benson, D.G., and Pratt, L.M., 2008, Anatomy of epicontinental flooding: late Albian–Early Cenomanian of the southern US Western Interior, *in* Pratt, B.R., and Holmden, C., eds., Dynamics of Epeiric Seas: Sedimentological, Paleontological and Geochemical Perspectives: Geological Association of Canada, Special Paper, v. 48, p. 201–227.

Otvos, E.G., 2000, Beach ridges: definitions and significance: Geomorphology, v. 32, p. 83–108.

Otvos, E.G., 2019a, Beach ridges, *in* Finkl, C.W., and Makowski, C., eds., Encyclopedia of Earth Sciences Series: Encyclopedia of Coastal Science, p. 290–296.

Otvos, E.G., 2019b, Cheniers, *in* Finkl, C.W., and Makowski, C., eds., Encyclopedia of Earth Sciences Series: Encyclopedia of Coastal Science, p. 290–296.

Pemberton, S.G., MacEachern, J.A., Dashtgard, S.E., Bann, K.L., Gingras, M.K., and Zonneveld, J.P., 2012, Shorefaces, *in* Knaust, D., and Bromley, R.G., eds., Elsevier, Developments in Sedimentology, v. 64, p. 563–603.

Plint, A.G., and Wadsworth, J.A., 2003, Sedimentology and palaeogeomorphology of four large valley systems incising delta plains, western Canada Foreland Basin: implications for mid-Cretaceous sea-level changes: Sedimentology, v. 50, p. 1147–1186.

Proisy, C., Gratiot, N., Anthony, E.J., Gardel, A., Fromard, F., and Heuret, P., 2009, Mud bank colonization by opportunistic mangroves: a case study from French Guiana using lidar data: Continental Shelf Research, v. 29, p. 632–641.

Prost, M.T., 1989, Coastal dynamics and chenier sands in French Guiana: Marine Geology, v. 90, p. 259–267.

Reading, H.G., 1996, Sedimentary Environments: Processes, Facies and Stratigraphy, 3rd Edition: Boston, Blackwell Science, 688 p.

Reed, D.J., Davidson-Arnott, R., and Perillo, G.M., 2009, Estuaries, coastal marshes, tidal flats and coastal dunes: Geomorphology and Global Environmental Change, v. 30, p. 130–157.

Retallack, G.J., 1988, Field recognition of paleosols, *in* Reinhardt, J., and Sigleo, W.R., eds., Paleosols and Weathering Through Geologic Time: Principles and Applications: Geological Society of America, Special Paper 216, p. 1–20.

Retallack, G.J., 2001, Soils of the Past: An Introduction to Paleopedology, Second Edition: Blackwell Science, 600 p.

Retallack, G.J., Wolberg, D.L., Stump, E., and Rosenberg, G.D., 1997, Dinosaurs and dirt, *in* Wolberg, D.L., Stump E., and Rosenberg G.D., eds., DinoFest International, p. 345–359.

Reynolds, A.D., 1999, Dimensions of paralic sandstone bodies: American Association of Petroleum Geologists, Bulletin, v. 83, p. 211–229.

Roberts, E.M., 2007, Facies architecture and depositional environments of the Upper Cretaceous Kaiparowits Formation, southern Utah: Sedimentary Geology, v. 197, p. 207–233.

Roca, X., and Nadon, G.C., 2007, Tectonic control on the sequence stratigraphy of non-marine retroarc foreland basin fills: insights from the Upper Jurassic of central Utah, USA: Journal of Sedimentary Research, v. 77, p. 239–255.

Shimer, G.T., Benowitz, J.A., Layer, P.W., McCarthy, P.J., Hanks, C.L., and Wartes, M., 2016, $^{40}Ar/^{39}Ar$ ages and geochemical characterization of Cretaceous bentonites in the Nanushuk, Seabee, Tuluvak, and Schrader Bluff formations, North Slope, Alaska: Cretaceous Research, v. 57, p. 325–341.

Steel, R.J., Plink-Bjorklund, P., and Aschoff, J., 2012, Tidal deposits of the Campanian Western Interior Seaway, Wyoming, Utah and Colorado, USA, *in* Davis, R.A., and Dalrymple, R.W., eds., Principles of Tidal Sedimentology: Dordrecht, Springer, p. 437–471.

Stokes, W.L., 1952, Lower Cretaceous in Colorado Plateau: American Association of Petroleum Geologists, Bulletin, v. 36, p. 1766–1776.

Suarez, C.A., González, L.A., Ludvigson, G.A., Cifelli, R.L., and Tremain, E., 2012, Water utilization of the Cretaceous Mussentuchit Member local vertebrate fauna, Cedar Mountain Formation, Utah, USA: using oxygen isotopic composition of phosphate: Palaeogeography, Palaeoclimatology, Palaeoecology, v. 313, p. 78–92.

Suarez, C.A., Frederickson, J., Cifelli, R.L., Pittman, J.G., Nydam, R.L., Hunt-Foster, R.K., and Morgan, K., 2021, A new vertebrate fauna from the Lower Cretaceous Holly Creek Formation of the Trinity Group, southwest Arkansas, USA: PeerJ, v. 9, no.12242.

Suarez, M.B., González, L.A., and Ludvigson, G.A., 2011, Quantification of a greenhouse hydrologic cycle from equatorial to polar latitudes: the mid-Cretaceous water bearer revisited: Palaeogeography, Palaeoclimatology, Palaeoecology, v. 307, p. 301–312.

Suarez, M.B., Suarez, C.A., Al-Suwaidi, A.H., Hatzell, G., Kirkland, J.I., Salazar-Verdin, J., Ludvigson, G.A., and Joeckel, R.M., 2017, Terrestrial Carbon Isotope Chemostratigraphy in the Yellow Cat Member of the Cedar Mountain Formation: complications and pitfalls, *in* Zeigler, K.E., and Parker, W., eds., Terrestrial Depositional Systems: Deciphering Complexities through Multiple Stratigraphic Methods: Amsterdam, Elsevier, p. 303–336.

Tabor, N.J., and Myers, T.S., 2015, Paleosols as indicators of paleoenvironment and paleoclimate: Annual Review of Earth and Planetary Sciences, v. 43, p. 333–361.

Tabor, N.J., Myers, T.S., and Michel, L.A., 2017, Sedimentologist's guide for recognition, description, and classification of paleosols, *in* Zeigler, K.E., and Parker, W.G., eds., Terrestrial Depositional Systems: Deciphering Complexities through Multiple Stratigraphic Methods: Amsterdam, Elsevier, p. 165–208.

Tagliapietra, D., Sigovini, M., and Ghirardini, A.V., 2009, A review of terms and definitions to categorise estuaries, lagoons and associated environments: Marine and Freshwater Research, v. 60, p. 497–509.

Tibert, N.E., Leckie, R.M., Eaton, J.G., Kirkland, J.I., Colin, J.P., Leithold, E.L., and McCormic, M.E., 2003, Recognition of relative sea level change in Upper Cretaceous coal-bearing strata: a paleoecological approach using agglutined foraminifera and ostracodes to detect key stratigraphic surfaces, *in* Olson, H., and Leckie, R.M., eds., Microfossils as a Proxy for Sea Level Changes and Stratigraphic Discontinuities: SEPM, Special Publication 75, p. 263–299.

Tucker, R.T., Roberts, E.M., Darlington, V., and Salisbury, S.W., 2017, Investigating the stratigraphy and palaeoenvironments for a suite of newly discovered mid-Cretaceous vertebrate fossil localities in the Winton Formation, Queensland, Australia: Sedimentary Geology, v. 358, p. 210–229.

Tucker, R.T., Zanno, L.E., Huang, H.Q., and Makovicky, P.J., 2020, A refined temporal framework for newly discovered fossil assemblages of the upper Cedar Mountain Formation (Mussentuchit Member), Mussentuchit Wash, central Utah: Cretaceous Research, v. 110, no. 104384.

Vail, P.R., Mitchum, R.M., Jr., Todd, R.G., Widmier, J.M., Thompson, S., III, Sangree, J.B., Bubb, J.N., and Hatlelid, W.G., 1977, Seismic stratigraphy and global changes of sea level: Part 4. Global cycles of relative changes of sea level, *in* Payton, C.E., ed., Seismic Stratigraphy: Application of Seismic Reflection Configuration to Stratigraphic Interpretation: American Association of Petroleum Geologists, Memoir 26, p. 49–212.

Wang, Y., Healy, T., Augustinus, P., Baba, M., Bao, C., Flemming, B., Fortes, M., Han, M., Marone, E., Mehta, A., and Ke, X., 2002, Definition, properties, and classification of muddy coasts, *in* Healy, T., Wang, Y., and Healy, J.A., eds., Muddy Coasts of the World: Processes, Deposits and Function: Elsevier, Proceedings in Marine Science 4, p. 9–18.

Wang, Y., Huang, C., Sun, B., Quan, C., Wu, J., and Lin, Z., 2014, Paleo-CO_2 variation trends and the Cretaceous greenhouse climate: Earth-Science Reviews, v. 129, p. 136–147.

Ward, C.R., 2002, Analysis and significance of mineral matter in coal seams: International Journal of Coal Geology, v. 50, p. 135–168.

Weleschuk, Z.P., and Dashtgard, S.E., 2019, Evolution of an ancient (Lower Cretaceous) marginal-marine system from tide-dominated to wave-dominated deposition, McMurray Formation: Sedimentology, v. 66, p. 2354–2391.

Welton, B.J., and Farish, R.F., 1993, The collectors guide to fossil sharks and rays from the Cretaceous of Texas: Before Time, 204 p.

White, T.S., Witzke, B.J., and Ludvigson, G.A., 2000, Evidence for an Albian Hudson arm connection between the Cretaceous western interior seaway of North America and the Labrador Sea: Geological Society of America, Bulletin, v. 112, p. 1342–1355.

White, T., Witzke, B., Ludvigson, G., and Brenner, R., 2005, Distinguishing base-level change and climate signals in a Cretaceous alluvial sequence: Geology, v. 33, p. 13–16.

Willis, G.C., 1999, The Utah thrust system: an overview, *in* Spangler, L.W., and Allen, C.J., eds., Geology of Northern Utah and Vicinity: Utah Geological Association, Publication 27, p. 1–9.

Winkler, D.A., Murry, P.A., and Jacobs, L.L., 1990, Early Cretaceous (Comanchean) vertebrates of central Texas: Journal of Vertebrate Paleontology, v. 10, p. 95–116.

Whybrow, P.J., and McClure, H.A., 1980, Fossil mangrove roots and palaeoenvironments of the Miocene of the eastern Arabian Peninsula: Palaeogeography, Palaeoclimatology, Palaeoecology, v. 32, p. 213–225.

Yingling, V.L., and Heller, P.L., 1992, Timing and record of foreland sedimentation during the initiation of the Sevier orogenic belt in central Utah: Basin Research, v. 4, p. 279–290.

Zakaria, R., 2016, A study of open coast tidal flat sedimentology based on outcrop data in Ngrayong Formation, Kadiwono Area, Central Java: Seminar Nasional Kebumian, Peran Penelitian Ilmu Kebumian Dalam Pemberdayaan, Proceedings.

Zanno, L.E., and Makovicky, P.J., 2013, Neovenatorid theropods are apex predators in the Late Cretaceous of North America: Nature Communications, v. 4, p. 1–9, doi:10.1038/ncomms3827.

Zanno, L.E., Tucker, R.T., Canoville, A., Avrahami, H.M., Gates, T.A., and Makovicky, P.J., 2019, Diminutive fleet-footed tyrannosauroid narrows the 70-million-year divergence in the North American fossil record: Communications Biology, v. 2, no. 64.

Zeng, Z., Pike, M., Tice, M.M., Kelly, C., Marcantonio, F., Xu, G., and Maulana, I., 2018, Iron fertilization of primary productivity by volcanic ash in the Late Cretaceous (Cenomanian) Western Interior Seaway: Geology, v. 46, p. 859–862.

Zhou, J., Poulsen, C.J., Pollard, D., and White, T.S., 2008, Simulation of modern and middle Cretaceous marine $\delta^{18}O$ with an ocean–atmosphere general circulation model: Paleoceanography, v. 23, p. 1–11.

Zubalich, R., Capozzi, R., Fanti, F., and Catuneanu, O., 2021, Evolution of the Western Interior Seaway in west-central Alberta (late Campanian, Canada): implications for hydrocarbon exploration: Marine and Petroleum Geology, v. 124, no. 104779.

Received 17 March 2021; accepted 6 April 2022.